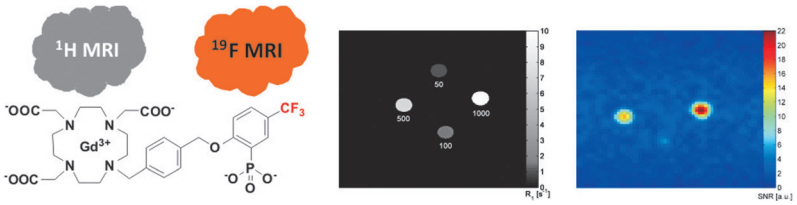

Sealed in a dual: The unusually high relaxivities of a series of macrocyclic lanthanide complexes were investigated, revealing a combination of rapid water exchange rates with a significant influence of water in the second sphere. Fluorine-containing complexes could be visualized by ^{1}H and ^{19}F MR phantom imaging (see figure); these platforms are promising candidates for dual frequency MRI.

Imaging Agents

*M. P. Placidi, M. Botta, F. K. Kálmán, G. E. Hagberg, Z. Baranyai, A. Krenzer, A. K. Rogerson, I. Tóth, N. K. Logothetis, G. Angelovski** ..... ▮▮▮▮–▮▮▮▮

Aryl-Phosphonate Lanthanide Complexes and Their Fluorinated Derivatives: Investigation of Their Unusual Relaxometric Behavior and Potential Application as Dual Frequency ^{1}H/^{19}F MRI Probes

CHEMISTRY
A EUROPEAN JOURNAL

ChemPubSoc
Europe

DOI: 10.1002/chem.201300763

Aryl-Phosphonate Lanthanide Complexes and Their Fluorinated Derivatives: Investigation of Their Unusual Relaxometric Behavior and Potential Application as Dual Frequency $^{1}H/^{19}F$ MRI Probes

Matteo P. Placidi,[a] Mauro Botta,[b] Ferenc K. Kálmán,[c] Gisela E. Hagberg,[a, d] Zsolt Baranyai,[c] Andreas Krenzer,[e] Alexandria K. Rogerson,[f] Imre Tóth,[c] Nikos K. Logothetis,[a, g] and Goran Angelovski*[a]

Abstract: A series of low molecular weight lanthanide complexes were developed that have high ^{1}H longitudinal relaxivities (r_1) and the potential to be used as dual frequency ^{1}H and ^{19}F MR probes. Their behavior was investigated in more detail through relaxometry, pH-potentiometry, luminescence, and multinuclear NMR spectroscopy. Fitting of the ^{1}H NMRD and ^{17}O NMR profiles demonstrated a very short water residence lifetime (<10 ns) and an appreciable second sphere effect. At lower field strengths (20 MHz), two of the complexes displayed a peak in r_1 (21.7 and 16.3 $mM^{-1}s^{-1}$) caused by an agglomeration, that can be disrupted through the addition of phosphate anions. NMR spectroscopy revealed that at least two species are present in solution interconverting through an intramolecular binding process. Two complexes provided a suitable signal in ^{19}F NMR spectroscopy and through the selection of optimized imaging parameters, phantom images were obtained in a MRI scanner at concentrations as low as 1 mM. The developed probes could be visualized through both ^{1}H and ^{19}F MRI, showing their capability to function as dual frequency MRI contrast agents.

Keywords: fluorine · gadolinium · imaging agents · NMR spectroscopy · relaxivity

Introduction

Molecular imaging involves the detection of specific metabolites or biochemical processes at the cellular level, enabling the early detection of diseases and dysfunctions by examining the underlying causes.[1] Of the many different imaging modalities considered, magnetic resonance imaging (MRI) shows great promise, providing noninvasive anatomical images with high spatiotemporal resolution at unlimited depths of tissue penetration. Its diagnostic ability relies on the differences in the longitudinal (T_1) and transverse (T_2) relaxation times of healthy and diseased tissue. Paramagnetic complexes are applied to improve the image quality reducing the relaxation times of the tissues in which they localize.[2] The vast majority administered in clinical settings are T_1 agents based on chelates of Gd^{3+}, chosen because of its favorable magnetic properties. The efficacy of a contrast agent is measured in terms of longitudinal relaxivity (r_1), defined as the increase in the observed longitudinal relaxation rate of the surrounding water protons normalized to its concentration. The relaxivity arises from the time-dependent magnetic coupling between the paramagnetic metal ion and the protons of the surroundings water molecules. These can be grouped in three main categories: the water molecules directly coordinated to the metal ion (inner sphere; IS), those diffusing in close proximity (outer sphere; OS), and those interacting with the ligand structure (second sphere; SS) for example, through hydrogen bonding.

[a] Dr. M. P. Placidi, Dr. G. E. Hagberg, Prof. Dr. N. K. Logothetis, Priv.-Doz. Dr. G. Angelovski
Department for Physiology of Cognitive Processes
Max Planck Institute for Biological Cybernetics
72076 Tuebingen (Germany)
E-mail: goran.angelovski@tuebingen.mpg.de

[b] Prof. Dr. M. Botta
Dipartimento di Scienze e Innovazione Tecnologica
University of Piemonte Orientale "Amedeo Avogadro"
15121 Alessandria (Italy)

[c] Dr. F. K. Kálmán, Dr. Z. Baranyai, Prof. Dr. I. Tóth
Department of Inorganic and Analytical Chemistry
University of Debrecen, 4010 Debrecen (Hungary)

[d] Dr. G. E. Hagberg
Biomedical Magnetic Resonance, Department of Radiology
Tuebingen University Hospital, 72076 Tuebingen (Germany)

[e] A. Krenzer
Department of Chemistry, Faculty of Science
University of Tuebingen, 72076 Tuebingen (Germany)

[f] A. K. Rogerson
The School of Chemistry
University of Manchester, Manchester M13 9PL (UK)

[g] Prof. Dr. N. K. Logothetis
Department of Imaging Science and Biomedical Engineering
University of Manchester, Manchester M13 9PT (UK)

Supporting information for this article is available on the WWW under http://dx.doi.org/10.1002/chem.201300763.

Further progress in this direction has been hindered by the inherent drawbacks associated with these agents—the high detection limit and uncertainty regarding quantification and localization. To lower the detection limit, their effectiveness can be improved by the development of high-relaxivity agents. This requires tuning of the microparameters that govern their inner sphere relaxivity, as described by the Solomon–Bloembergen–Morgan treatment of paramagnetic relaxation.[3] These include slowing the rotation of the chelate (τ_R), decreasing the bound water residence lifetime (τ_M), or increasing the number of directly coordinated water molecules (q).[4] Portions of the ligand can also be used to enhance the population of water molecules in the second sphere, leading to an increase of r_1.[5] Replacing one of the carboxylate arms of **GdDOTA** with a methyl phosphonate as in **GdDO3AP**, led to a reduction of τ_M and the presence of two water molecules in the second sphere, thus causing an increase in r_1.[6] A number of studies in the past two decades have focused on the development of effective, high-relaxivity agents.[7]

The indirect detection of these agents results in difficulties in interpreting their exact location and concentration, as other intrinsic processes of the surrounding tissue also affect the image contrast for example, hemorrhaging, inflammation or lesions.[8] To overcome this issue significant research has been devoted to developing agents with a different MR active nucleus where the measured signal is directly related to the concentration of the substance, as in the case of radioisotope imaging agents. ^{19}F is ideally suited to this role as the amount of fluorine in the soft tissues is insignificant resulting in no interfering background signals. Also, it has a very similar gyromagnetic ratio to ^{1}H, allowing the use of the same experimental setup to record both signals from each subject. By combining the ^{19}F image and the ^{1}H anatomical scan, much more detailed information can be obtained. This has already been exploited to examine melanoma angiogenesis or quantify and monitor the fates of implanted stem and dendritic cells.[9] Most investigations have used perfluorinated nanoemulsions, however these systems have inherently long relaxation times (the order of seconds), which results in longer scan times. Also, some contain multiple fluorine resonances that lead to a low signal intensity, thus requiring high concentrations to obtain a suitable signal. To overcome these issues, multiple fluorinated units have been incorporated on macromolecules such as polymers or dendrimers, though their high molecular weight restricts them to the vasculature.[10] Alternatively, using a paramagnetic relaxation enhancement (PRE) effect, a paramagnetic ion can be incorporated in close proximity to ^{19}F, thus reducing the relaxation times by several orders of magnitude, increasing the signal-to-noise ratio by enabling more scans within shorter periods of time.[11] In this direction researchers have developed systems that are able to detect enzyme activity,[12] or a series of lanthanide chelates with CF_3 groups at optimized geometries to obtain an effective signal detected at μM concentrations.[13]

Agents able to satisfy the demands of the two MRI methods and produce both strong ^{1}H and ^{19}F signals are rare. They include either a mixture of molecules encapsulated in micelles[14] or self assembled structures.[15] While these systems are effective, there is a desire to produce small, single molecule agents with optimal dual frequency signals, by combining a high-relaxivity agent with a ^{19}F containing group which can take advantage of the PRE effect due to the proximity of the paramagnetic ion.

We have previously developed a series of macrocyclic ligands appended with an aryl-phosphonate moiety, suited for both MR and optical imaging.[16] The relaxivities of these probes at high magnetic field strengths (7 T) were greater than expected for low weight Gd^{3+} complexes, more than twice that of commercial agents. In addition to understanding the factors influencing their behavior, we sought to prepare and investigate the properties of four new agents, each containing a CF_3 moiety incorporated at different positions (Figure 1). The distance and orientation of the ^{19}F nucleus

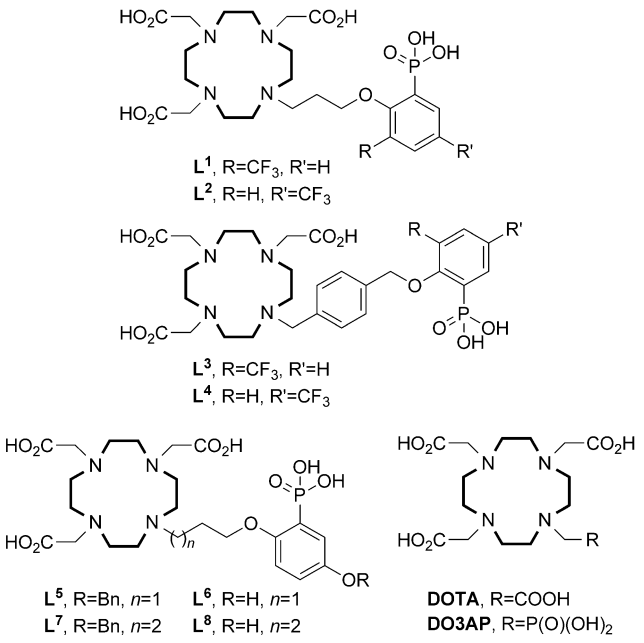

Figure 1. Structures of ligands **L**$^{1-8}$, **DOTA**, and **DO3AP**.

with respect to the Ln^{3+} ion is of critical importance in determining the strength of the ^{19}F signal.[17] Therefore, we coupled the fluorinated aryl moiety to the macrocycle using both a rigid and flexible linking unit, varying the position of the CF_3 group on the aromatic ring. Furthermore we sought to analyze the best candidates in MRI phantoms, through the use of new imaging parameters with the ultimate goal of developing a platform for dual frequency $^{1}H/^{19}F$ MR imaging.

Results and Discussion

Ligand synthesis: The synthesis of the four new ligands $\mathbf{L^{1-4}}$ followed a similar route to $\mathbf{L^{5-8}}$ (Figure 2),[16] the main difference involved the construction of the multifunctional aromatic moiety. The MR active CF_3 group was incorporated either *ortho* or *para* to the phenol ether, hence the phosphonate was introduced by treating 2- or 4-triflouromethyl phenol (**1a**,**b**) with diethyl phosphite to give **2a** and **2b**, respectively. A Phospho-Fries rearrangement using LDA at −78 °C, induced an *ortho* migration of the phosphonate resulting in **3a** and **3b**. 1,3-dibromopropane and 1,4-bis(bromomethyl)benzene were monoalkylated with both **3a** and **3b** to give the bromides **4a–d**. Here, the higher reactivity of the xylyl-derivative necessitated its addition in a large excess under high dilution conditions. The tris *tert*-butyl ester derivative of cyclen was then treated with **4a–d** and the ligand precursors **5a–d** were isolated using column chromatography on alumina, in high yields. The two different ester protecting groups were cleaved sequentially, first using bromotrimethylsilane in *N*,*N*-dimethylformamide and then trifluoroacetic acid in dichloromethane. ^{1}H NMR spectroscopy and mass spectrometry confirmed the removal of the protecting groups and each ligand ($\mathbf{L^{1-4}}$) was purified using RP-HPLC (see Tables S1–S3 in the Supporting Information for the conditions) and lyophilized.

The lanthanide complexes were prepared through the slow addition of an equimolar amount of the corresponding chloride salt to an aqueous solution of the ligand at 60 °C, while maintaining the pH at 6–7 using sodium hydroxide. Once the free ligands could no longer be detected through mass spectrometry, the excess lanthanide ions were removed by precipitation from solution at pH 10, followed by treatment of the supernatant with Chelex. The absence of free lanthanide ions was confirmed using the xylenol orange test.

Lanthanide luminescence: The luminescence properties of $\mathbf{EuL^{1-4}}$ and $\mathbf{TbL^{1-4}}$ were examined by recording the excitation and emission spectra (Figures S1–S4 in the Supporting Information). For each of the Tb^{3+} systems a strong ligand based transition could be observed in the UV region and excitation of this resulted in intense green emission centered at 545 nm. In addition to the ligand excitation band, $\mathbf{EuL^{1-4}}$ displayed a sharp peak at 395 nm of similar intensity, corresponding to an f–f transition originating from the metal ion. Excitation at either wavelength resulted in the same Eu^{3+} emission spectra centered at 617 nm. The observation of this additional excitation peak indicates a reduced efficiency of the sensitized emission process relative to the Tb^{3+} complexes. Given the electron-rich nature of the chromophore, it is likely that the Eu^{3+} emissive state is being partially deactivated by a low-lying ligand to metal charge transfer state, previously observed in other Eu^{3+} phenol-containing complexes.[18] The nature of the other substituents on the aromatic ring influences this quenching process to differing extents, such that in $\mathbf{EuL^{1-4}}$ sensitized emission is inefficient and in $\mathbf{EuL^{5-8}}$ it is not observed.

Table 1. Luminescence lifetimes[a] and hydration numbers of $\mathbf{EuL^{1-8}}$ and $\mathbf{TbL^{1-8}}$.[b]

Complex	Tb^{3+}			Eu^{3+}		
	τD_2O [ms][c]	τH_2O [ms][c]	q	τD_2O [ms][d]	τH_2O [ms][d]	q
$\mathbf{L^1}$	3.07	1.65	1.1	1.92	0.54	1.3
$\mathbf{L^2}$	3.28	1.83	0.9	1.90	0.60	1.1
$\mathbf{L^3}$	2.78	1.63	1.1	1.73	0.64	0.9
$\mathbf{L^4}$	2.83	1.60	1.1	1.77	0.58	1.1
$\mathbf{L^5}$	3.40	2.01	0.7	1.73	0.58	1.1
$\mathbf{L^6}$	3.23	1.97	0.7	0.80	0.36	1.5
$\mathbf{L^7}$	3.10	1.90	0.7	0.97	0.47	1.0
$\mathbf{L^8}$	3.04	2.20	0.3	0.76	0.37	1.3

[a] Lifetimes quoted are subject to a ±10% error. [b] Data for $\mathbf{TbL^{5-8}}$ from ref. [16]. [c] λ_{ex} = 285–300 nm, λ_{em} = 545 nm. [d] λ_{ex} = 395 nm, λ_{ex} = 617 nm.

When considering the available amino carboxylate donor set, q is expected to be either 1 or 2 depending on if the phosphonate is bound to the metal ion or not. This can be determined from the luminescence lifetimes recorded in H_2O and D_2O (MOPS, pH 7.4), and by applying the modified Horrocks' equation (Table 1).[19] The lifetimes were measured either through excitation of the chromophore (Tb^{3+}, λ_{ex} = 285–300 nm) or by direct excitation of the metal ion (Eu^{3+}, λ_{ex} = 395 nm). For $\mathbf{EuL^{1-8}}$ the hydration numbers ranged from 1–1.5 suggesting that the phosphonate is connected to the metal ion. This is supported by the splitting pattern of the $\Delta J = 1$ manifold and the peak at 620 nm, ob-

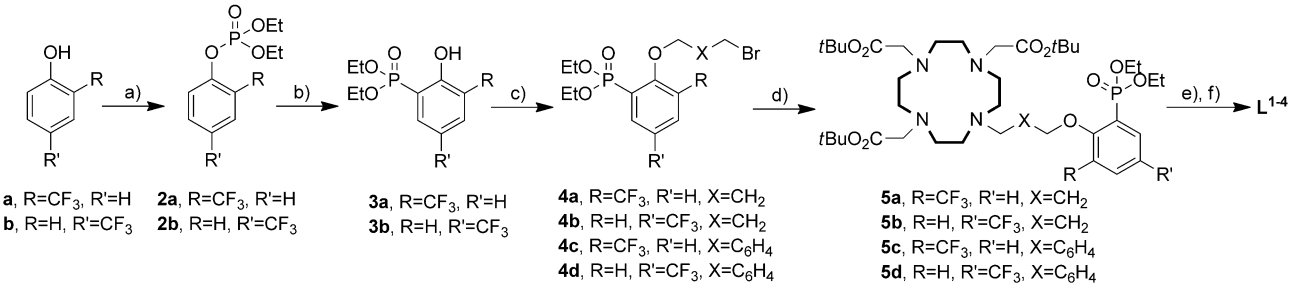

Figure 2. Synthetic scheme for $\mathbf{L^{1-4}}$: a) $HP(O)(OEt)_2$, Et_3N, CCl_4; b) LDA, THF, −78 °C; c) dibromopropane or *p*-dibromoxylene, K_2CO_3, DMF, 60 °C; d) tris-*t*Bu-DO3A, K_2CO_3, CH_3CN or DMF, 70 °C; e) Me_3SiBr, DMF; f) TFA, CH_2Cl_2.

served in the emission spectra.[20] The noninteger values may represent a mixture of mono- and bis-hydrated species (with the phosphonate in bound and unbound positions respectively). It is also possible that the higher q values of **EuL**^{6} and **EuL**^{8} are a result of the stronger electron donating nature of the phenol substituent, enhancing the charge transfer quenching pathway and providing an overestimation of q. **TbL**$^{1-7}$ are all monohydrated, the slightly lower q values are likely a result of the smaller ionic radii of Tb^{3+} compared to Eu^{3+}. The main exception is **TbL**^{8} with a q value close to 0, which seems reasonable given that the relaxivity of the **GdL**^{8} is lower than the other Gd^{3+} complexes (see below).

Table 2. Relaxometric parameters for **GdL**$^{1-8}$ obtained from the fit of the ^{1}H NMRD profiles and ^{17}O NMR data.

Gd^{3+} chelates	r_1 [mM^{-1}s^{-1}][a]	Δ^2 [10^{19} s^{-2}]	τ_V [Ps]	τ_R [Ps]	τ_M [ns][b]	$\Delta H_M^{\#}$ [kJ mol^{-1}][b]	$A/\hbar$ [10^{6} rad s^{-1}][b]
L^{1}	7.6	1.6 (3.0)[c]	40 (27)[c]	164 (148)[c]	16 (15)[c]	33.8 (31.6)[c]	−3.7 (−3.7)[c]
L^{2}	7.4	2.1	34	143	8	10	–
L^{3}	21.7 (8.4)[d]	1.3 (2.6)[d]	49 (29)[d]	568 (166)[d]	10 (12)[d]	– (17.2)[d]	– (−3.5)[d]
L^{4}	16.3 (8.6)[d]	2.1 (2.4)[d]	40 (32)[d]	430 (168)[d]	10 (11)[d]	– (18.1)[d]	– (−3.6)[d]
L^{5}	7.7	2.0	35	155	8.5	26.0	−3.5
L^{6}	7.9	2.0 (4.1)[c]	39 (24)[c]	154 (142)[c]	8.1 (8.3)[c]	25.6 (25.3)[c]	−3.5 (−3.5)[c]
L^{7}	6.9	2.6	27	131	10	–	–
L^{8}	6.3	2.5	27	108	7.2	34.1	−3.4
DOTA[e]	4.7	1.6	11	77	243	49.8	−3.6

[a] Recorded at 20 MHz and 25 °C. [b] Values obtained from the fitting of VT ^{17}O NMR spectra. [c] Values obtained by including the second sphere contribution in the fitting of the ^{1}H NMRD profile. [d] Values obtained from fitting of the ^{1}H NMRD profile in 200 mM PBS. [e] Ref. [23b].

Relaxometric characterization: The longitudinal proton relaxivities of **GdL**$^{1-8}$ were determined at 20 MHz, 25 °C and neutral pH by measuring the longitudinal relaxation times, with two sets of values observed; 6.3–7.9 mM^{-1}s^{-1} for **GdL**$^{1-2,5-8}$ and 16.3–21.7 mM^{-1}s^{-1} for **GdL**^{3,4} (Table 2). In the first group there is an increase in r_1 with increasing molecular weight, in line with a reduction in the tumbling rate (Figure S5 in the Supporting Information). **GdL**^{1} and **GdL**^{6} have slightly elevated values given their hydration numbers ($q=1$), indicating an additional contribution to r_1, likely due to the presence of a significant number of second sphere water molecules, previously observed for other phosphonate containing systems.[21] The elevated values of **GdL**^{3,4} are similar to those found in slow tumbling macromolecular systems.[22] The r_1 was measured as a function of pH (4–9), with each complex displaying constant values (Figures S6–S9 in the Supporting Information) indicating the hydration state and hence the coordination environment is not significantly affected at this pH range. As demonstrated previously for **GdL**$^{5-8}$, the carbonate anions present at high pH do not interfere by displacing the inner sphere water molecules. At pH 3, a steady increase was observed indicating the partial dissociation of the complex and ultimately the release of the metal ion. The temperature dependence of r_1 was also measured for three of the complexes (**GdL**^{1}, **GdL**^{3}, and **GdL**^{4}) resulting in an exponential increase in r_1 with decreasing temperature—a typical behavior for rapidly exchanging systems (Figures S10 and S11 in the Supporting Information). Here, the water exchange rates ($k_{ex}=1/\tau_M$) are much shorter than the longitudinal relaxation time of the bound water (T_{1M}) and hence will not limit the overall relaxivities.

NMRD profiles: The relaxometric behavior of **GdL**$^{1-8}$ was investigated in more detail by recording nuclear magnetic resonance dispersion (NMRD) profiles (Figure 3 and Figures S12–S15 in the Supporting Information).[23] Through fitting of the NMRD profiles using the standard equations that describe inner and outer sphere relaxivity, a series of microparameters can be obtained (Table 2).[4a] For the data analysis it is necessary to make a reasonable estimate of some of the parameters: q was fixed to 1; the Gd-inner sphere water proton distance $r=3.0$ Å, the Gd-outer sphere water–proton distance $a=4.0$ Å, the diffusion coefficient $D=2.24\times10^{-5}$ cm^{2}s^{-1} (25 °C). For each system increasing the temperature from 25 to 37 °C, decreased r_1 over the entire frequency range investigated (0.01–70 MHz), indicating a stronger influence of τ_R over τ_M. **GdL**$^{1-2,5-8}$ displayed typical behavior for monometallic chelates with a single dispersion at 1–7 MHz. The highest r_1 values were observed at

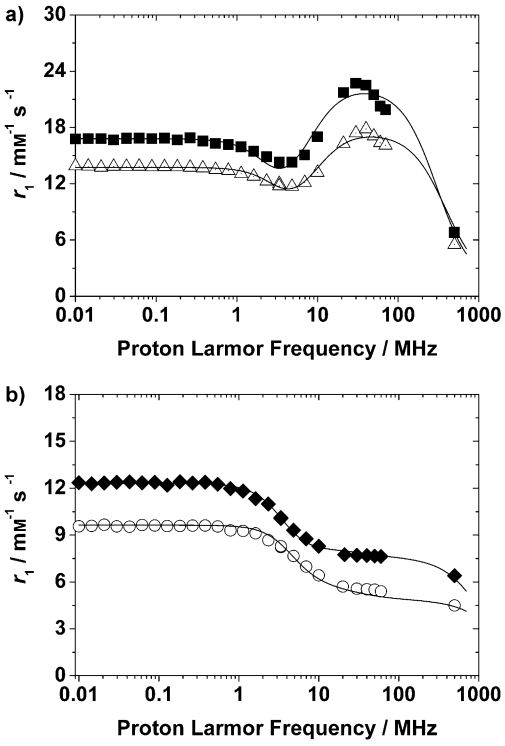

Figure 3. a) ^{1}H NMRD profiles of **GdL**^{3} (■) and **GdL**^{4} (△) in water at 25 °C; b) **GdL**^{5} in water at 25 (◆) and 37 °C (○).

lower magnetic field strengths, with similar values to **GdDOTA**.[4a,24]

Over this range r_1 is known to be strongly influenced by the electronic relaxation rates ($1/T_{ie}$), described by the trace of the square of the zero-field splitting tensor, Δ^2 and the correlation time describing its modulation, τ_V. The Δ^2 values are much closer to **GdDOTA** than **GdDO3A**,[23b,25] supporting the predominance of a $q=1$ species and hence the coordination of the phosphonate arm. At higher field strengths r_1 decreases, coinciding with the region where the τ_R strongly influences r_1, a result of the rapid tumbling rate of the complex, though the τ_R values obtained for **GdL$^{1-2,5-8}$** are twice that of **GdDOTA** at 150 ps.[26] The linear increase of r_1 with molecular weight observed with most of these compounds, combined with the occurrence of $q=1$ and the τ_R values calculated suggest that the phosphonate arm is most likely bound to the metal center. If the phosphonate arm remained unbound, the flexible solution state structure would result in lower τ_R values for molecules of this molecular weight.

The large peak in r_1 measured at 30–40 MHz in the NMRD profiles of **GdL^{3,4}** is indicative of a slow tumbling species, observed previously for many high molecular weight systems.[27] The τ_R of 568 and 430 ps were obtained for **GdL^{3,4}**, however, due to the presence of more than one species in solution (see below) these values can only be considered in a qualitative sense. Given the available donor set and the rigid nature of the xylyl linking unit, it appears that two or more complexes are associating together to form slower diffusing dimers or oligomers. This effect has been observed previously by Merbach et al., who found a series of xylyl-linked macrocyclic complexes to agglomerate in solution, providing high τ_R and r_1 values.[28]

This likely involves hydrophobic π–π stacking and/or hydrogen bonding interactions between the aromatic cores and the macrocyclic binding sites respectively. To test this hypothesis we recorded the NMRD profiles of **GdL^{3,4}** and **GdL^{1}** (as a control) in a solution of PBS containing either a standard or excess amount of phosphate anions (previously shown to break down such aggregates).[28] Should these interactions be disrupted, then the form of the profiles would alter and the peak in the slow tumbling region should decrease or disappear. A reduction in the peak height can clearly be observed in the slow tumbling region in the presence of 10 mM phosphate (Figures S16 and S17 in the Supporting Information), with the change being more prominent for **GdL^{4}**. The lesser effect on **GdL^{3}** suggests that the agglomeration is much stronger, which is reasonable given that its r_1 in the absence of PBS is higher. On addition of 200 mM phosphate the peak completely disappears, with the form and intensity of the profiles resembling that of the other monomeric complexes. Accordingly, the best-fit parameters assume standard values (Table 2). We previously observed that the r_1 of **GdL^{1}** and **GdL^{6}** appear sensibly higher than typical values for monohydrated Gd^{3+} complexes of similar molecular size (Figure S5 in the Supporting Information).

This can be explained by the presence of a non-negligible contribution from second sphere water molecules, not uncommon in the case of Gd^{3+} chelates functionalized with hydrophilic pendant groups. In this case we reanalyzed the data by considering three additional parameters: τ_R' (r_1^{SS}; in the range 20–80 ps) and q'/r' (r_1^{SS}). A very good fit was obtained by considering the contribution of two water molecules ($q'=2$), located at a distance of 3.8 Å from the metal ion with a rotational correlation time of approximately 30–35 ps (Figures S12 and S14 in the Supporting Information). Clearly, this type of analysis is mainly qualitative as a network of water molecules located at different distances from the metal ion and with different lifetimes contribute collectively to the overall relaxivity. However, it provides a reasonable explanation for the unusual values of relaxivity and more accurate relaxation parameters. In fact, all the NMRD profiles have been analyzed assuming either the presence of a single water molecule ($q=1$) in the inner sphere of the metal ion and the occurrence of contributions to r_1 from inner- and outer sphere components only. One method to check if q has been assigned correctly is to plot the calculated rotational correlation time, τ_R, versus the molecular weight of the complexes (Figure 4). According to the

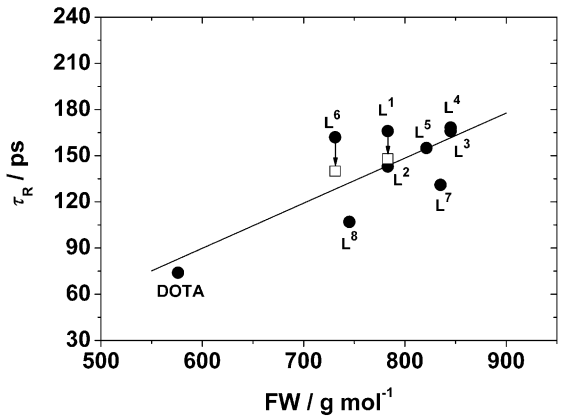

Figure 4. Rotational correlation time, τ_R, versus molecular weight for **GdDOTA** and for the complexes discussed in the present work. Open symbols refer to the τ_R values after refining the NMRD profiles with inclusion of the second sphere relaxivity (**GdL^{1,6}**).

Debye–Stokes equation, a linear relationship should be found for rigid spherical molecules with negligible internal motion. It is clear that a good linear correlation is obtained for **GdL$^{2-5}$**. For **GdL^{1,6}** the calculated τ_R are too large, but fall on the straight line after consideration of the second sphere contribution. On the other hand, for **GdL^{7,8}** the calculated τ_R appear to be underestimated and this is likely the result of the compensation for a lower effective q value. Both **GdL^{7,8}** values follow the Debye–Stokes relationship more closely if q is set to approximately 0.9. Another possible explanation for the deviation from linearity in the case of **GdL^{7,8}** may be the presence of an anisotropic molecular rotation which results in a lower "effective" correlation time τ_R.

Variable temperature ^{17}O NMR: Variation of τ_M between 5–50 ns provided the same degree of fitting for the NMRD profiles. Therefore, the transverse relaxation rates (R_{2p}) and shift ($\Delta\omega$) of the ^{17}O nucleus were recorded as a function of temperature for a selection of complexes (Figure 5 and Figures S18–S22 in the Supporting Information) and τ_M could be accurately determined by application of the Swift–Connick equations.[29] Again, some parameters were fixed to standard values: $q=1$, the activation energy of the correlation time for the modulation of the transient zero-field-splitting tensor $E_V=1.5$ kJ mol^{-1} and the activation energy of the rotational correlation time $E_R=18$ kJ mol^{-1}. In addition, for Δ^2 and τ_V the values derived from the fit of the NMRD profiles were used. The variable parameters were: the mean residence lifetime of the inner sphere water molecule τ_M, its enthalpy of activation $\Delta H_M^{\#}$, and the scalar Gd–^{17}O$_w$ coupling constant $A/\hbar$.

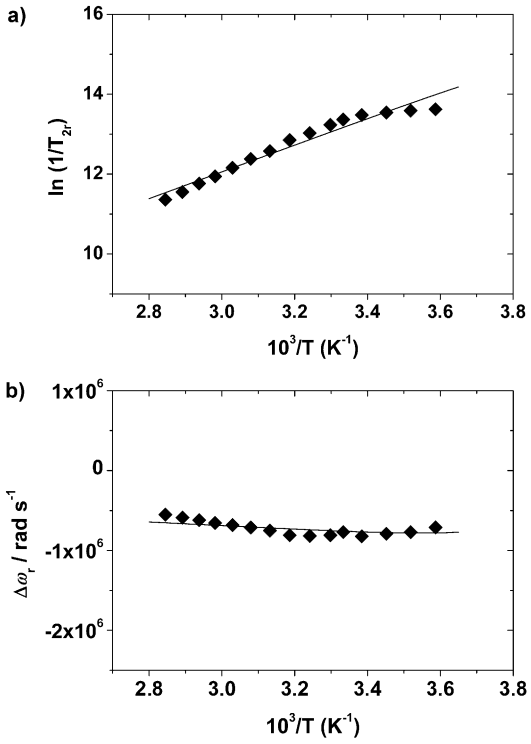

Figure 5. Reduced transverse: a) ^{17}O relaxation rates, and b) ^{17}O chemical shifts of an aqueous **GdL^5** (19.2 mM, 11.75 T, neutral pH).

An exponential increase in R_{2p} is observed with decreasing temperature for each system demonstrating their rapid exchange of water with the surrounding bulk, to the extent that the peak in R_{2p} which corresponds to the crossover between the slow and fast exchange cannot be observed. A τ_M of approximately 8 ns was obtained for each system studied (Table 2) in the range observed previously for other phosphonate appended macrocyclic systems. It is likely that the presence of the bulky phosphonate group is causing steric crowding around the metal ion, increasing the rate of exchange.[6,21b,25]

Table 3. Protonation constants of **L^1**, **L^3**, and **L^8** (0.15 M NaCl, 25 °C).

	L^1	**L^3**	**L^8**	**DOTA**[a]
$\log K_1^H$	9.89 (1)	9.41 (2)	10.67 (1)	9.14
$\log K_2^H$	9.88 (2)	9.26 (2)	10.06 (1)	9.21
$\log K_3^H$	7.09 (4)	7.17 (3)	9.64 (1)	4.48
$\log K_4^H$	4.25 (5)	4.53 (4)	7.72 (2)	4.03
$\log K_5^H$	3.61 (4)	3.37 (4)	4.25 (3)	1.99
$\log K_6^H$	1.79 (4)	2.15 (4)	3.52 (2)	–
$\log K_7^H$	–	–	2.00 (1)	–
$\Sigma\log K_i^H$	36.50	35.88	47.86	28.85

[a] Ref. [32].

Protonation equilibria: The protonation constants of **L^{1,3,8}** ($\log K_i^H$) were determined by pH-potentiometric titrations (Table 3, the definitions and equations used for the evaluation of the equilibrium data are summarized in the Supporting Information). The $\log K_i^H$ values of these ligands differ considerably from those of **DOTA**, which can be explained in part by the different protonation sequences. The protonation Scheme of **DOTA** has been studied in detail, where the first two take place at the transannular macrocyclic amines and the remaining three correspond to the carboxylate arms.[30] The protonation sequences of **L^{1,3}** are similar to each other, the first and second steps correspond to the two ring amines, the third, fourth, fifth, and sixth protonations occur at the phosphonate and the carboxylate groups, respectively. At very acidic conditions the phosphonate group is expected to undergo a further protonation,[31] which could not be accurately determined by direct pH-potentiometric titrations. For **L^8**, the first protonation takes place at the phenol, the second and third are related to the macrocyclic amines. The fourth protonation of **L^8** involves the phosphonate group and the remaining three take place at the carboxylate groups.

The $\log K_i^H$ values of the amines in the macrocyclic ring for **L^{1,8}** are significantly higher than those of **L^3** and **DOTA**, to the extent that the $\log K_2^H$ of the former are higher than the $\log K_1^H$ values of the latter. The higher amine $\log K_i^H$ values of **L^{1,8}** may be due to the following effects: 1) the electron donating and withdrawing effects of the alkyl (**L^{1,8}**) versus aromatic (**L^3**) linkers on the ring N-atom, which increases the basicity, 2) a stronger complex formation between the fully deprotonated ligands (**L^3**) and sodium ion which reduce the proton affinity of the ring N-atoms, 3) a greater degree of electrostatic repulsion between the protonated ring N-atoms (**L^3**), and 4) the potential barrier for the formation of a H-bonding interaction between the protonated nitrogen atom and the carboxylate group increasing the basicity of amines (**L^{1,8}**). The $\log K_i^H$ of the phosphonate group occurs at a range of values similar to that measured previously for other aryl-phosphonate derivatives[31] and the $\log K_i^H$ values of the carboxylic groups are comparable in all cases.

Complexation properties: It is well established that di- and trivalent metal ions form very stable complexes with **DOTA** and its derivatives, due to the coordination cage formed by

the four ring nitrogen and four carboxylate oxygen donor atoms. The stability constants of the Ln^{3+} complexes **L**[1,3,8] (which possess four N- and three carboxylate O-donor atoms) are expected to be lower than those of **DOTA**. However, given the solution-state behavior described in the previous sections, the influence of the aryl-phosphonate pendant arm on the coordination with the metal center cannot be ruled out. The formation of Ln^{3+} complexes with **DOTA** and its derivatives is slow at the pH range 3–6, because the entrance of the Ln^{3+} ion into the cage formed by the donor atoms is hindered. The two macrocyclic nitrogens are protonated forming an intermediate $*LnH_2DOTA$ in the first step of the complexation (the stability constant of the intermediate can be defined as $*K_{\mathbf{LnH_2L}}=[*LnH_2L]/[Ln^{3+}][H_2L]$). This slowly deprotonates with the rate determining step involving the loss of the second proton[33] (here the stability constants were determined using the "out-of-cell" technique, because of the slow rate of complex formation). The use of separate samples in these measurements leads to larger errors in $\log K_{\mathbf{GdDOTA}}$ resulting in a wide range of values (22.1–28.0) in the literature.[34] These large discrepancies may also be attributed the use of very different measurement techniques employed (pH-potentiometry, direct spectrophotometry, competition with Arsenaso III, spectrofluorometry, and solubility). Therefore, to accurately determine the stability constants of the Gd^{3+} complexes, the proton relaxation rates of Gd^{3+} (0.002 M) in the presence of **L**[1,8] (0.002 M) were measured over the pH range 2.0–3.4 (Figure S23 in the Supporting Information).

In addition to free Gd^{3+} and **GdL**[1,8], the intermediates $*\mathbf{GdH_4L}$[1] and $*\mathbf{GdH_3L}$[8] are also present at low concentrations (4–20%). These intermediates contribute significantly to r_1 due to the presence of 4–5 water molecules occupying their inner-sphere. In $*\mathbf{GdH_4L}$[8] two diagonal ring nitrogens, the phenolate and phosphonate groups are protonated and hence unable to coordinate, in $*\mathbf{GdH_3L}$[1] two diagonal ring nitrogens and the phosphonate group are protonated. The stability constants of **GdL**[1,8] were calculated by using the r_1 of the $Gd^{3+}_{aq.}$ ion, $\mathbf{GdH_2L}$[8], **GdHL**[1], and the intermediates $*\mathbf{GdH_4L}$[8] and $*\mathbf{GdH_3L}$[1], which were determined in separate experiments (see Table S4 in the Supporting Information for the r_1 of each intermediate). The protonation constants were also determined by pH-potentiometric titrations for **GdL**[1,8], whereas the precipitation of $\mathbf{GdH_2L}$[3] prevented an accurate protonation constant determination.

The stability and protonation constants of Ca^{2+}, Zn^{2+}, and Cu^{2+} complexes of **L**[1,3,8] were investigated by pH-potentiometric titrations (Table 4), and the stability constants of **CuL**[1,3,8] were determined by spectrophotometry (Figure S24; the absorption spectra and the equations used for the evaluation of the equilibrium data are summarized in the Supporting Information). The stability constants of the Ca^{2+} and Gd^{3+}-complexes of **L**[1,3,8] are lower than those of the corresponding **DOTA** complexes, whereas the values for the Zn^{2+} and Cu^{2+} complexes are comparable or higher. The smaller $\log K_{ML}$ values of the Ca^{2+} and Gd^{3+} complexes can be explained in terms of the higher coordination number (CN) of the metal ions and the lower denticity of **L**[1,3,8]. The coordination requirements of Zn^{2+} and Cu^{2+} (CN 6), can be fully saturated by the 7 donor atoms. Moreover, it is possible that **L**[1,8] have a more suitable cavity size for Zn^{2+} and Cu^{2+}, resulting in higher stability constants. Interestingly, the lower denticity of **CuL**[1] resulting in a higher $\log K_{ML}$ value (when compared to **CuDOTA**) has also been observed with **CuDO3A** ($\log K_{\mathbf{CuDO3A}}=26.49$, 0.5 M KNO_3, 25 °C).[38] Since the basicity of the N-donor atoms of **L**[1], DO3A and DOTA ligands are very similar, it can be assumed that the higher stability of the **CuL**[1] complex is caused by the optimal coordination geometry of the macrocyclic donor atoms for the Cu^{2+}, due to the presence of the aromatic substituent on the ring N-atom.

Table 4. Stability and protonation constants of the Ca^{2+}, Zn^{2+}, Cu^{2+} and Gd^{3+} complexes of **L**[1], **L**[3] and **L**[8] (0.15 M NaCl, 25 °C).

	L[1]	**L**[3]	**L**[8]	**DOTA**
CaL	**10.26 (4)**	**10.07 (6)**	**9.43 (2)**	**13.84 (1)**
CaHL	7.32 (3)	7.12 (5)	10.63 (2)	3.90 (2)
CaH_2L	–	–	8.18 (1)	–
ZnL	**18.66 (4)**	**16.98 (2)**	**17.95 (3)**	**17.35 (1)**
ZnHL	7.25 (3)	7.11 (2)	10.55 (3)	4.16 (2)
ZnH_2L	3.86 (2)	3.99 (2)	8.13 (2)	3.40 (1)
ZnH_3L	2.99 (1)	2.97 (2)	4.10 (1)	2.65 (1)
ZnH_4L	–	–	2.96 (1)	–
CuL[a]	**22.56 (2)**	**21.17 (4)**	**21.75 (3)**	**22.00**[b]
CuHL	7.11 (1)	6.96 (3)	10.50 (1)	4.08
CuH_2L	4.07 (1)	3.84 (4)	8.02 (3)	3.41
CuH_3L	2.63 (2)	2.21 (4)	4.27 (4)	0.83
CuH_4L	1.74 (2)	1.80 (4)	2.63 (3)	–
CuH_5L	–	–	2.12 (4)	–
GdL[c]	**18.3 (1)**	–	**19.0 (1)**	**24.7**[d]/**22.4**[e]
GdHL	6.86 (2)	–	10.15 (2)	–
GdH_2L	–	–	6.92 (4)	*5.9 (Eu^{3+})[f]
$*GdH_3L$[g]	5.25 (8)	–	–	–
$*GdH_4L$[g]	–	–	5.51 (5)	–

[a] Determined by VIS-spectrophotometry; the ionic strength was not constant. [b] Ref. [32]. [c] Determined by relaxometry (0.15 M NaCl, 25 °C). [d] Ref. [35] (0.1 M NaCl, 25 °C). [e] Ref. [36] (0.1 M NaCl 25 °C). [f] Stability constant of the Eu(H_2DOTA) intermediate.[33a,37] [g] Stability constant of intermediate (0.15 M NaCl, 25 °C).

Overall the stability constants of the Ca^{2+}, Zn^{2+}, Cu^{2+}, and Gd^{3+}-complexes indicate that the presence of the aryl-phosphonate pendant arm and its potential interaction with the metal center does not significantly improve the stability of the complex. Indeed, the protonation of the Ca^{2+}, Zn^{2+}, and Cu^{2+} complexes formed with **L**[1,3,8] takes place at a similar or slightly higher pH than that of the corresponding ligands (Table 4), thereby indicating the absence of an interaction between the aryl-phosphonate group and the metal ions. This is also seen in the further protonation constants of the Zn^{2+} and Cu^{2+} complexes of **L**[1,3,8] that involve the non-coordinated carboxylate pendant arms. However, the Gd^{3+} complexes behave differently—all protonation constants (of the phosphonate group in **GdL**[1] or both, the phenol and the phosphonate group in **GdL**[8]) are lower than those of the respective ligands **L**[1,8] (Tables 3 and 4). The more acidic nature of the phosphonate group in a Ln^{3+} complex has also occurred in other phosphonate appended systems in which

this group interacts with Gd^{3+}.[36,39] These observations indicate that a similar process takes place in **GdL^{1,8}**, supporting the above differences in stability constants of the investigated metal complexes, and a result of the higher CN of Gd^{3+}.

Dissociation kinetics: To further assess the potential stability of a Gd^{3+} complex in vivo, the kinetic inertness of **GdL^{1,3,8}** was investigated. The dissociation of the metal complexes in vivo can occur either when endogenous metal ions (Ca^{2+}, Zn^{2+} or Cu^{2+}) compete with the Gd^{3+} for the ligand or more rarely, by competition of endogenous ligands for Gd^{3+}. The effect of a tenfold excess of Cu^{2+} was investigated by spectrophotometry in the pH range 3–5 and the kinetic inertness of the metal complexes was characterized by the rate constants of the exchange reactions with the endogenous metal ion. The excess Cu^{2+} ensures the reaction can be regarded as pseudo-first-order and the rate of the reaction can be expressed by Equation (1), where k_d is the pseudo-first-order rate constant and $[GdL]_{tot}$ is the total concentration of the Gd^{3+} complex.

$$-\frac{d[GdL]}{dt} = k_d[GdL]_{tot} \quad (1)$$

Over the pH range 3–5, **GdL^{8}** exists predominantly in the diprotonated form, whereas **GdL^{1}** forms a monoprotonated species. The equilibrium stability and protonation constants of **GdL^{3}** could not be determined owing to its low solubility, therefore it was assumed that only the phosphonate moiety is protonated. The decomplexation reactions of the Gd^{3+} complexes can occur via spontaneous, proton assisted and metal assisted pathways (Scheme S1 in the Supporting Information). The k_d values of the metal exchanging reactions increase linearly with the H^+ concentration. It has been found that the role of the exchanging metal ion is negligible in this initial process, so the dissociation of the complexes can take place via spontaneous and proton assisted pathways, followed by the fast reaction between the free ligand and the exchanging metal ion. Taking into account these possible pathways and considering that $[\mathbf{GdL^8}]_{tot} = [\mathbf{GdH_2L^8}] + [\mathbf{GdH_3L^8}]$ and $K_{\mathbf{GdH_3L^8}} = [\mathbf{GdH_3L^8}]/[\mathbf{GdH_2L^8}][H^+]$, furthermore $[\mathbf{GdL^{1,3}}]_{tot} = [\mathbf{GdHL^{1,3}}] + [\mathbf{GdH_2L^{1,3}}]$ and $K_{\mathbf{GdH_2L^{1,3}}} = [\mathbf{GdH_2L^{1,3}}]/[\mathbf{GdHL^{1,3}}][H^+]$, the rate constants characterizing the spontaneous and proton assisted dissociation can be given by Equations (2) and (3), where k_0 characterizes the spontaneous decomplexation and k_1 is the fist-order rate constant of the proton assisted dissociation of **GdH$_2$L^{8}** and **GdHL^{1,3}**.

$$k_d = \frac{k_0 + k_1[H^+]}{1 + K^H_{GdH_2L^8}[H^+]} \quad (2)$$

$$k_d = \frac{k_0 + k_1[H^+]}{1 + K^H_{GdHL^{1,3}}[H^+]} \quad (3)$$

The proton assisted dissociation process most likely involves a proton transfer step from the phosphonate side arm to the nitrogen atom of the macrocyclic ring, followed by the loss of Gd^{3+}. The results of the best fit of the k_d values to Equations (2) and (3) are shown in Table 5 (see Figures S25–S27 in the Supporting Information for the dependence of k_d on $[H^+]$).

Table 5. The rate constants of the dissociation of **GdL^{1}**, **GdL^{3}**, and **GdL^{8}** (25 °C, 0.15 M NaCl).

	GdL^{1}	**GdL^{3}**	**GdL^{8}**	**GdDTPA**[a]	**GdDOTA**[b]
k_0 [s^{-1}]	$(1.3\pm0.4)\times10^{-5}$	–	–	–	6.7×10^{-11}
k_1 [$s^{-1}M^{-1}$]	8.5 ± 0.2	4.0 ± 0.1	5.2 ± 0.3	0.58	1.8×10^{-6}
K_H [M^{-1}]	–	190 ± 62	–	100	14

[a] Ref. [39]. [b] Ref. [40].

During the fitting process the k_0 values of the decomplexation of **GdH$_2$L^{8}** and **GdHL^{3}**, as well as the protonation constants of the intermediates $K_{\mathbf{GdH_3L^8}}$ and $K_{\mathbf{GdH_2L^3}}$ were found to be negligible (values are comparable with their standard deviation). The proton assisted dissociation rate of the investigated complexes is under one order of magnitude higher than that of **GdDTPA** and 2–3 times slower than **GdDTPA-BMA**,[41] MRI contrast agents frequently used in medical practice. However, it occurs several orders of magnitude quicker than that of **GdDOTA** and **GdDO3A**.[42] Previously the substitution of the carboxylate with a phosphonate group increased the rate of proton-assisted dissociation, as the phosphonate groups are readily protonated even in bound form, facilitating the proton transfer to the macrocyclic nitrogen.[43] The presence of the phosphonate moiety in the investigated ligands may help explain this lower kinetic inertness, given that the interaction between the phosphonate group and Gd^{3+} does not improve the thermodynamic stability of the complex (Table 4). It is possible that additional effects such as steric crowding and/or intermolecular dimerization are contributing to the destabilization of the complexes. However, the investigated complexes are suitable for further in vivo testing, as prototype contrast agents due to their similar kinetic inertness to agents such as **GdDTPA**.

NMR spectroscopy: Further information about the coordination environment of Ln-DOTA- or DO3A-type complexes can be obtained from NMR spectroscopy. The presence of a paramagnetic ion is expected to alter the width and position of the ^{31}P NMR peak, the extent of which is not only dependent on the lanthanide itself but also the distance and orientation of the NMR active nuclei with respect to this ion.[44] Eu^{3+} complexes are frequently used to determine the nature of the species present in solution, reflected in the number and position of the peaks. Given its proximity in the lanthanide series, Eu^{3+} is often used as a surrogate to provide information that cannot be obtained directly from the Gd^{3+} analogues. For **EuL$^{1-8}$** peaks in two regions at 10

to 15 and −90 to −150 ppm were observed (Figure 6 and Figures S28–S31 in the Supporting Information), the latter being significantly broader. This suggests that the phosphonate experiences two environments: one in close proximity to the paramagnetic ion, the other further away. We envisage a reversible binding process with different proportions of the phosphonate group free or coordinated to Eu^{3+}. When considering the form of the NMRD profiles and the τ_R of **GdL**$^{1,2,5-8}$ (Table 2), it appears that this occurs in an intramolecular fashion. Given the agglomeration observed for **GdL**^{3,4}, the exact nature of the process is more difficult to determine.

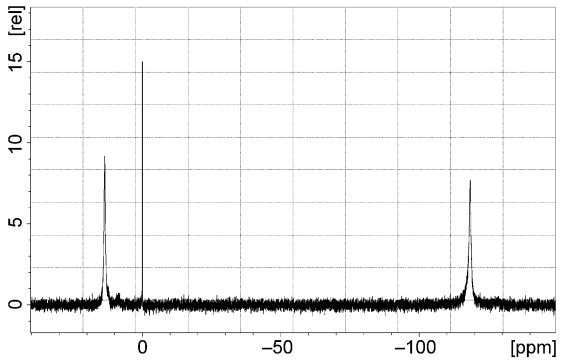

Figure 6. ^{31}P NMR spectra of **EuL**^{3} (25 °C, D_2O, 1 % H_3PO_4 external standard).

Lanthanide complexes of DOTA and its derivatives typically exist in solution as two interconverting stereoisomers: square antiprismatic (SAP) and twisted square antiprismatic (TSAP) geometries.[45] The isomers differ in terms of the angle between the two planes containing the four oxygen and four nitrogen coordinating atoms, that sit above and below the lanthanide ion (ca. 40 and 25° respectively).[46] The ^{1}H NMR spectra of **EuL**$^{1-8}$ displayed a series of broadened signals over a range of −40 to +40 ppm, characteristic of complexes of this ion (Figure 7 and Figures S32–S35 in the Supporting Information). Given the low symmetry of this system and DO3A derivatives in general, a signal for each proton is expected.[47] Attention is often focused on the axial protons of the macrocyclic ring as they experience the greatest shift to a region with fewer signals, enabling an easier interpretation of the species present. For **EuL**$^{3,6-8}$ only the SAP isomer was detected with four axial peaks in the region 20–50 ppm.[48] For the remaining complexes at least two species were observed corresponding to both SAP and TSAP isomers. When comparing the respective ^{1}H and ^{31}P NMR spectra, a single peak is present in the bound region (−90 to 150 ppm in ^{31}P NMR) when only the SAP isomer is present, whereas two or more signals are observed in this region when both SAP and TSAP isomers are detected.

For application in ^{19}F MRI the complex must give a suitable signal, ideally a single resonance in the corresponding ^{19}F NMR spectrum with T_1 and T_2 relaxation times compatible with the MR imaging pulse sequences. There are many factors that influence the number and proportion of isomers of lanthanide complexes in solution and hence the number of ^{19}F signals, including the choice of the lanthanide ion. Therefore, for each ligand **L**$^{1-4}$ a series of 4 different complexes (Eu^{3+}, Gd^{3+}, Tb^{3+}, and Yb^{3+}) were made and their ^{19}F NMR spectra were recorded. 14 of the complexes contained multiple peaks rendering them unsuitable, as this would reduce the overall signal intensity in MRI. However, for **GdL**^{4} and **YbL**^{4} a single broad signal was observed (Figure S36 in the Supporting Information) with T_1, T_2 times of 3.1, 2.0 and 272.8, 4.2 ms respectively, allowing them to be examined further in MRI phantom measurements (see below).

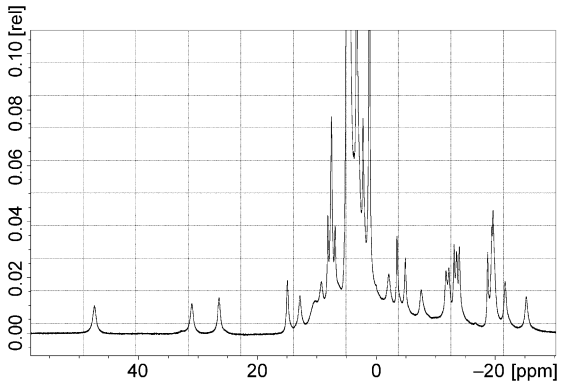

Figure 7. ^{1}H NMR spectra of **EuL**^{3} (25 °C, D_2O).

The agglomeration observed in the relaxometric analysis was examined using the diamagnetic Y^{3+} complexes of **L**^{1,3}, prepared as representatives of discrete and aggregating species respectively. ^{1}H DOSY NMR spectroscopy was used to determine the number of species in solution and the diffusion rate (D) as a function of the ^{1}H chemical shift (Figures S37–S39 in the Supporting Information). D is known to be dependent on the size and shape of a given species in solution[49] and it is expected that the formation of agglomerates will result in a reduction of this value. The aromatic region was examined in more detail as it contained fewer and better resolved signals for easier analysis, compared to the broader signals of the aliphatic protons undergoing rapid exchange processes. As expected, only one species could be observed for **YL**^{1} with a diffusion coefficient of 3×10^{-10} m^2s^{-1}, matching that of a monomacrocyclic complex of similar molecular weight (determined by PGSE ^{1}H NMR experiments).[50] For **YL**^{3} at least two species were observed with diffusion coefficients ranging from $1.5–2.3\times10^{-10}$ m^2s^{-1}, both diffusing at a slower rate than **YL**^{1}. It is likely that the slower diffusing species correspond to an intermolecular dimer and oligomer, supported by the behavior demonstrated in the NMRD profile. The DOSY NMR spectrum of **YL**^{3} was then re-measured in the presence of 200 mM PBS to examine the disruption of the agglomeration process (Figures S40 and S41 in the Supporting Information). Here a simplification of the spectrum can be observed with a reduction

in the number of signals, especially in the aromatic region with a diffusion coefficient of 2.0×10^{-10} m^2s^{-1}. This indicates a significant disruption of the aggregate, to a form that more closely resembles **YL**[1].

^{1}H and ^{19}F MRI phantom measurements: The imaging capabilities of these complexes were assessed in vitro, by recording ^{1}H MR phantom images of **GdL**[4] at various concentrations in MOPS buffered solution (10–80 μM), using a 7 T horizontal animal bore MRI scanner. As expected the presence of the complex caused a significant brightening of the image contrast, due to a reduction in the T_1 time of the surrounding water. In parallel, a series of dilutions of **GdDOTA** were also recorded at the same concentrations, and throughout this range **GdL**[4] is more readily observable, which is expected given its higher r_1 value (Figure S42 in the Supporting Information). ^{19}F MR images were recorded for both **YbL**[4] and **GdL**[4] which displayed a single broad signal (see above), with the same MRI scanner. For each complex a series of four buffered solutions at different concentrations (1–5 mM) were prepared to determine the detection limit of each system in vitro, which is related to the T_1 and T_2 times of both complexes. Using a FLASH sequence signals from both complexes could be observed, providing the images with a total collection time of 60 min. This sequence proved most effective for **YbL**[4] yielding a maximal signal-to-noise ratio (SNR) of 14 at 5 mM with similar SNR for the highest **GdL**[4] concentration (Figures 8a and b, respectively). Employing an alternative fast imaging FISP sequence,[51] a much stronger signal for **GdL**[4] could be obtained. In only 15 min a SNR similar to that from the FLASH sequence was achieved, with concentrations as low as 1 mM detected, providing a maximal SNR of 9 (Figure 8c).

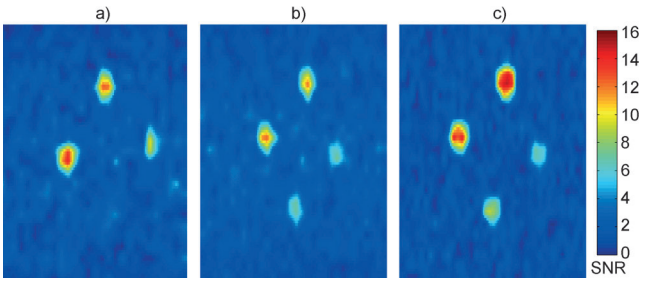

Figure 8. ^{19}F MRI phantom images of: a) **YbL**[4] using FLASH, b) **GdL**[4] recorded using FLASH, and c) FISP sequences; complex concentrations: a) 1.0 (bottom), 2.0 (right), 3.5 (left) and 5.0 mM (top); b,c) 1.0 (right), 2.0 (bottom), 3.5 (left), and 5.0 mM (top).

Since **GdL**[4] also has the potential to act as a dual frequency probe, further MR images were recorded at a lower range of concentrations (50–1000 μM). As expected, the shortest ^{1}H T_1 time and hence the brightest image resulted from the highest concentration of the complex, with an increase in T_1 with decreasing concentration. By altering the pulse sequence and tuning the receiver coil, complex concentrations as low as 0.1 mM could be observed in ^{19}F phantom images with an SNR above 3 in a 1 h acquisition time using the FISP sequence. The SNR of the 0.5 mM vial was 3–4 after 15 min (data not shown), representing the detection limit for the dual signal originating from this complex (Figure 9).

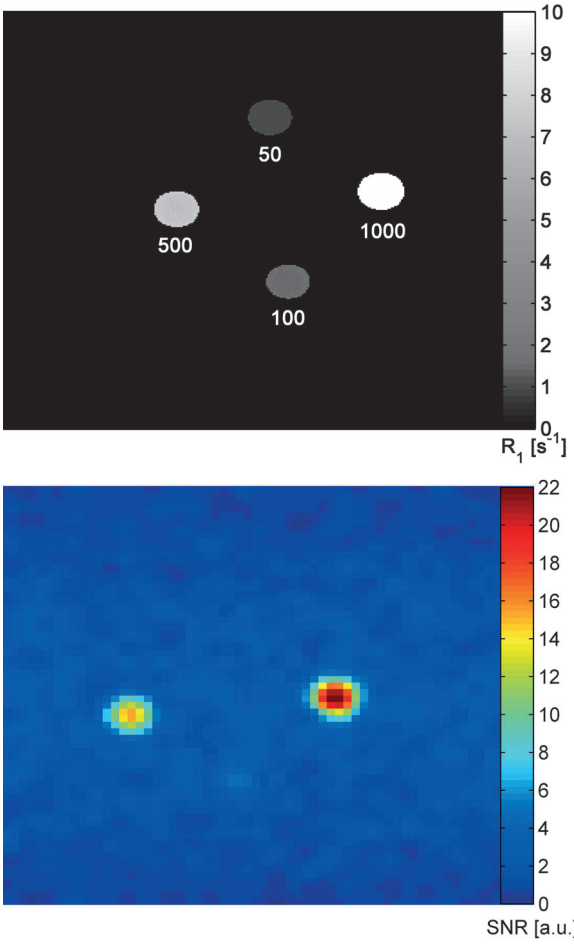

Figure 9. ^{1}H/^{19}F MR phantom images of **GdL**[4], recorded using an inversion recovery sequence and R_1 mapping by nonlinear least square fitting (^{1}H, top) and the FISP (^{19}F, bottom) sequence. The numbers in the ^{1}H MRI represent concentrations in μM.

Conclusion

Various physicochemical characteristics of a series of arylphosphonate macrocyclic complexes were investigated in more detail to understand the origins of their high r_1 and explore the potential for their use as dual frequency MRI contrast agents. Despite being monohydrated complexes, the enhanced r_1 appears to be the result of a comparatively slow rotation combined with a significant contribution from water molecules residing in the second hydration sphere. Furthermore, the fast rate of water exchange of these complexes will not limit their relaxivity at low temperatures or represent a limiting factor of r_1 in the case of their macromolecular conjugates.[52] Additionally, two of the complexes

displayed a peak in the ^{1}H NMRD profiles, at magnetic field strengths typically associated with slow tumbling macromolecular assemblies. This suggests that an agglomeration process is occurring, which was confirmed by ^{1}H DOSY NMR spectroscopy. However, the agglomeration can be disrupted by the addition of phosphate ions returning the systems to their monomeric state. ^{31}P NMR spectroscopy revealed that the phosphonate arm was reversibly binding to the metal ion creating two distinct environments in solution. The pH-potentiometry showed the expected protonation pattern of the ligands, whereas a reduction in the protonation constant for the phosphonate groups upon formation of the corresponding Gd^{3+} complexes supported the idea of the binding interaction. Furthermore, the complexes show a similar demetallization rate to that of **GdDTPA** rendering them suitable for further in vivo characterization for example, in preclinical studies. The possibility of one of the systems to be used as an MRI contrast agent was investigated through phantom measurements, where the ^{19}F signals from both the Yb^{3+} and Gd^{3+} complexes could be readily observed. Moreover, the Gd^{3+} complex showed the prospect of serving as a dual frequency ^{1}H/^{19}F probe, being detected at concentrations as low as 0.1 mM. This study demonstrates the potential for these agents to be developed into multifunctional MRI probes that induce MR signals at two frequencies and provide a plenitude of critical information gathered simultaneously from both ^{1}H and ^{19}F MRI.

Experimental Section

Synthesis: All chemicals were purchased from commercial sources and used without further purification, with the exception of THF, which was distilled prior to use. Tris *tert*-butyl-DO3A was prepared according to previously published procedures.[53] Column chromatography was performed using silica gel 60 (70–230 mesh ASTM) or aluminum oxide 90 active basic from Merck (Germany). Reversed-phase high-performance liquid chromatography was performed on a Varian PrepStar Instrument (Australia), equipped with PrepStar SD-1 pump heads. Analytical RP-HPLC was performed on an Atlantis C18 column 4.6 mm × 150 mm, particle size 5 μM, using method A (Table S1 in the Supporting Information). Preparative RP-HPLC was performed on an Atlantis C18 column 19 mm × 150 mm, particle size 5 μM, Waters corporation (USA) using method B and C (Tables S2 and S3 in the Supporting Information).

Diethyl 2-(trifluoromethyl)phenyl phosphate (2a): 2-(Trifluoromethyl) phenol **1a** (5.00 g, 30.8 mmol) was dissolved in carbon tetrachloride (30 mL) and this was cooled to 0 °C, triethylamine (5.37 mL, 38.6 mmol) and diethyl phosphite (4.93 mL, 38.6 mmol) were added. After warming the solution to room temperature a white precipitate formed and this was left to stir at this temperature overnight. Water was added followed by dichloromethane and the organic phase was washed with HCl (1 M), saturated sodium chloride solution, dried over sodium sulphate and the solvent was removed under reduced pressure. The crude product was purified using column chromatography (silica gel, from 9:1 to 1:1 hexane/ethyl acetate). Removal of the solvent yielded **2a** as a light yellow oil (8.89 g, 97 %). Tlc: R_f = 0.32 (silica, hexane/ethyl acetate = 7:3); ^{1}H NMR (300 MHz, $CDCl_3$): δ = 1.33 (td, $J_{H,H}$ = 7.2, 1.1 Hz, 6H; OCH_2CH_3), 3.99–4.24 (m, 4H; OCH_2CH_3), 7.20 (t, $J_{H,H}$ = 7.9 Hz, 1H; Ar*H*), 7.54–7.59 (m, 2H; Ar*H*), 7.60 ppm (m, 2H; Ar*H*); ^{13}C{^{1}H} NMR (75 MHz, $CDCl_3$): δ = 15.80 (d, $J_{C,P}$ = 6.6 Hz; OCH_2CH_3), 64.89 (d, $J_{C,P}$ = 6.6 Hz; OCH_2CH_3), 120.21(Ar*C*H), 121.17 (Ar*C*), 124.19 (Ar*C*H), 124.72 (q, $J_{C,F}$ = 5.5 Hz; *C*CF_3), 128.33 (Ar*C*H), 133.35 (Ar*C*H), 148.55 ppm (Ar*C*); ^{19}F{^{1}H} NMR (282 MHz, $CDCl_3$,): δ = −61.76 ppm; ^{31}P{^{1}H} NMR (122 MHz, $CDCl_3$): δ = −7.92 ppm, ESI-MS (pos.): *m*/*z*: 299 $[M+H]^+$, 321 $[M+Na]^+$, 337 $[M+K]^+$; HRMS (EI): *m*/*z*: calcd for $C_{11}H_{14}O_4F_3P_1$: 298.05818; found: 298.06175.

Diethyl 2-hydroxy-3-(trifluoromethyl) phenylphosphonate (3a): A flask containing the phosphate ester **2a** (4.30 g, 14.42 mmol) was purged of air and kept under dinitrogen, dry tetrahydrofuran (30 mL) was added and the solution was cooled to −78 °C. A solution of lithium diisopropylamine also under a dinitrogen atmosphere was prepared over 30 min by dissolving diisopropylamine (10.18 mL, 72.15 mmol) in tetrahyrofuran (20 mL) and cooling this to −78 °C, followed by the addition of *n*-butyl lithium (45.10 mL, 1.6 M, 72.15 mmol). This was then transferred via cannula to the phosphate solution, which changed the solution to a caramel color. After 3 h saturated ammonium solution was added to quench the reaction and the solution was warmed to room temperature. The product was extracted into diethyl ether; the organic phase was washed with saturated sodium chloride solution and dried over sodium sulphate. The solvent was removed under reduced pressure and the crude product was purified using column chromatography (silica gel, from 9:1 to 3:7 hexane/ethyl acetate). On removal of the solvent **3a** was isolated as an orange liquid (3.34 g, 78 %). Tlc: R_f = 0.69 (silica, EtOAc/hexane = 3:7); ^{1}H NMR (300 MHz, $CDCl_3$,): δ = 1.31 (t, 6H, $^3J_{H,H}$ = 7.0 Hz; $POCH_2CH_3$), 3.99–4.24 (m, 4H; $POCH_2CH_3$), 6.94–7.00 (m, 1H; Ar*H*), 7.52–7.59 (m, 1H; Ar*H*), 7.71 (d, 1H, $^3J_{H,H}$ = 7.7 Hz; Ar*H*), 11.02 ppm (s, 1H; PhO*H*); ^{13}C{^{1}H} NMR (75 MHz, $CDCl_3$,): δ = 15.98 (d, $J_{C,P}$ = 6.6 Hz; OCH_2CH_3), 63.11 (d, $J_{C,P}$ = 5.0 Hz; OCH_2CH_3), 109.82 (Ar*C*H), 112.23 (Ar*C*H), 118.77 (Ar*C*H), 125.00 (Ar*C*), 132.35 (q, $J_{C,F}$ = 2.2 Hz; *C*CF_3), 135.52 (Ar*C*), 160.00 ppm (Ar*C*); ^{19}F{^{1}H} NMR (282 MHz, $CDCl_3$): δ = −63.22 ppm; ^{31}P{^{1}H} NMR (122 MHz, $CDCl_3$): δ = 20.55 ppm; ESI-MS (pos.): *m*/*z*: 299 $[M+H]^+$, 321 $[M+Na]^+$, 337 $[M+K]^+$, (neg.): *m*/*z*: 297 $[M-H]^+$; HRMS (EI): *m*/*z*: calcd for $C_{11}H_{14}O_4F_3P_1$: 298.05818; found: 298.05505.

Diethyl 2-(3-bromopropoxy)-3-(trifluoromethyl) phenylphosphonate (4a): The phenol **3a** (2.0 g, 6.71 mmol) was dissolved in anhydrous dimethylformamide (20 mL) and potassium carbonate (1.85 g, 13.41 mmol) was added, this was heated to 60 °C for 1 hour under a dinitrogen atmosphere, changing the solution to a brown color. Dibromopropane (2.05 mL, 20.19 mmol) was added dropwise and the mixture was heated for a further 17 h. After cooling to room temperature the inorganic salts were removed by filtration and dichloromethane was added. The organic phase was washed with saturated sodium chloride solution and dried over sodium sulphate, and the solvent was removed under reduced pressure. The crude product was purified using column chromatography (silica gel, from 9:1 to 4:6 hexane/ethyl acetate). Removal of the solvents yielded **4a** as a light yellow liquid (2.26 g, 81 %). Tlc: R_f = 0.49 (silica, EtOAc/hexane = 1:1); ^{1}H NMR (300 MHz, $CDCl_3$): δ = 1.36 (t, 6H, $^3J_{H,H}$ = 7.0 Hz; $POCH_2CH_3$), 2.43 (quin, 2H, $^3J_{H,H}$ = 6.4 Hz; $BrCH_2CH_2$), 3.63 (t, 2H, $^3J_{H,H}$ = 7.0 Hz; $BrCH_2CH_2CH_2$), 4.12–4.25 (m, 4H; $POCH_2CH_3$), 4.30 (t, 2H, $^3J_{H,H}$ = 5.9 Hz; $BrCH_2$), 7.28–7.33 (m, 1H; Ar*H*), 7.80 (d, 1H, $^3J_{H,H}$ = 7.0 Hz; Ar*H*), 7.99–8.07 ppm (m, 1H; Ar*H*); ^{13}C{^{1}H} NMR (75 MHz, $CDCl_3$): δ = 16.10, 29.33, 33.36, 62.40, 74.89, 121.10, 123.85, 124.86, 126.39, 131.62, 138.47, 159.28 ppm; ^{19}F{^{1}H} NMR (282 MHz, $CDCl_3$) δ = −60.40 ppm; ^{31}P{^{1}H} NMR (122 MHz, $CDCl_3$): δ = 14.38 ppm; ESI-MS (pos.): *m*/*z*: 420 $[M+H]^+$, 442 $[M+Na]^+$; HRMS (EI): *m*/*z*: calcd for $C_{14}H_{20}O_4F_3P_1Br_1$: 420.013596; found: 420.01163.

Tri-*tert*-butyl 2,2′,2″-(10-(3-(2-(diethoxyphosphoryl)-6-(trifluoromethyl)-phenoxy)propyl)-1,4,7,10-tetraazacyclododecane-1,4,7-triyl)triacetate (5a): Tris *tert*-butyl-DO3A (2.80 g, 4.70 mmol), the phosphonate arm **4a** (2.96 g, 7.05 mmol) and potassium carbonate (1.95 g, 14.10 mmol) were dissolved in acetonitrile (40 mL) and the mixture was heated to 70 °C under a dinitrogen atmosphere. After 48 h the solution was cooled to room temperature, the inorganic salts were removed by filtration and the solvent was evaporated under reduced pressure. The resulting yellow oil was dissolved in dichloromethane and washed with saturated sodium chloride solution, dried over sodium sulphate and the solvent evaporated. The crude product was purified using column chromatography (alumina from 100 % dichloromethane to 96:4 dichloromethane/methanol). On removal of the solvents **5a** was obtained as a yellow solid (3.19 g, 80 %).

Tlc: R_f=0.53 (alumina, dichloromethane/methanol=92.5:7.5); ^{1}H NMR (300 MHz, $CDCl_3$): δ=1.35 (t, 6H, $^3J_{H,H}$=7.0 Hz; $POCH_2CH_3$), 1.43–1.45 (m, 27H; CCH_3), 1.96–4.25 (br m, 34H; CH_2 ring, NCH_2COO, $NCH_2CH_2CH_2O$, $POCH_2CH_3$), 7.30–7.33 (m, 1H; Ar*H*), 7.79 (d, 1H, $^3J_{H,H}$=7.7 Hz; Ar*H*), 7.94–8.04 ppm (m, 1H; Ar*H*); ^{13}C{^{1}H} NMR (75 MHz, $CDCl_3$): δ=15.89, 27.35, 49.73, 50.24, 51.67, 51.77, 55.31, 56.20, 62.00, 74.91, 80.19, 81.96, 82.32, 123.57, 123.75, 125.99, 131.31, 137.98, 159.19, 170.50, 172.15, 172.99 ppm; ^{19}F{^{1}H} NMR (282 MHz, $CDCl_3$): δ=−60.24, −60.27, −60.29, −60.36 ppm; ^{31}P{^{1}H} NMR (122 MHz, $CDCl_3$): δ=13.45, 14.05 ppm; ESI-MS (pos.): *m*/*z*: 853.5 $[M+H]^+$, 875.4 $[M+Na]^+$; HRMS (FT-ICR): *m*/*z*: calcd for $C_{40}H_{69}F_3N_4O_{10}P_1$: 853.46979 $[M+H]^+$; found: 853.46590.

2,2′,2″-(10-(3-(2-Phosphono-6-(trifluoromethyl)phenoxy)propyl)-1,4,7,10-tetraazacyclododecane-1,4,7-triyl)triacetic acid (L^1): The ester **5a** (1.2 g, 1.41 mmol) was dissolved in dimethylformamide (3 mL), this was cooled to 0 °C in an ice bath and bromotrimethylsilane (1.86 mL, 1.41 mmol) was added dropwise to the solution. This was warmed to room temperature and stirred for 18 h. The solvent was evaporated under reduced pressure and the removal of the ethyl groups was confirmed through electrospray mass spectrometry. A mixture of dichloromethane and trifluoroacetic acid (1:1, 10 mL) was added to the crude orange oil and the mixture was stirred at room temperature for 48 h. Following removal of the solvents a brown oil was obtained and electrospray mass spectrometry again confirmed the removal of the *tert*-butyl groups. The crude product was purified through reverse phase HPLC. On freeze drying L^1 was isolated as a flocculent white solid that quickly became a yellow oil due to its hygroscopic nature (0.746 g, 82%). ^{1}H NMR (300 MHz, D_2O): δ=2.24–4.20 (br m, 28H; CH_2 ring, NCH_2COO, $NCH_2CH_2CH_2O$,), 7.23 (m, 1H; Ar*H*), 7.68 (d, $^3J_{H,H}$=7.7 Hz, 1H; Ar*H*), 7.83–7.93 ppm (m, 1H; Ar*H*), ^{13}C{^{1}H} NMR (75 MHz, D_2O): δ=15.75, 23.34, 31.29, 36.80, 47.92, 48.18, 48.29, 49.63, 51.36, 52.44, 53.37, 56.34, 72.81, 121.82, 123.95, 130.21, 132.49, 137.72, 157.29, 164.78, 169.69, 173.06, 174.45 ppm; ^{19}F{^{1}H} NMR (282 MHz, D_2O): δ=−60.10, −60.13, −60.19, −60.22 ppm; ^{31}P{^{1}H} NMR (122 MHz, D_2O): δ=7.39, 9.47 ppm; ESI-MS (pos.): *m*/*z*: 629.3 $[M+H]^+$, 657.3 $[M+Na]^+$; HRMS (FT-ICR): *m*/*z*: calcd for $C_{24}H_{35}F_3N_4O_{10}P_1$: 627.20484 $[M-H]^-$; found: 627.20454.

2,2′,2″-(10-(3-(2-Phosphono-6-(trifluoromethyl)phenoxy)propyl)-1,4,7,10-tetraazacyclododecane-1,4,7-triyl)triacetic acid lanthanide complex (LnL^1): All the complexes were prepared according to the following procedure: The ligand ($\mathbf{L^{1-4}}$) and 1 equivalent of the lanthanide chloride were dissolved in water. The solution was heated to 70 °C and the pH was raised from 2–3 to 5–6 using sodium hydroxide (1 M) solution. This temperature and pH was maintained over a period of 24 h. After cooling to room temperature the excess lanthanide ions were removed by raising the pH to 10 and treating the supernatant with chelex-100. The xylenol orange test was used to confirm the absence of any free lanthanide ions in solution. The water was removed under reduced pressure to yield a yellow solid.

YL^1: ESI-MS (neg.): *m*/*z*: 713.1 $[M-H]^-$. **EuL^1**: ^{1}H NMR (300 MHz, D_2O): δ=−20.70, −17.43, −15.31, −13.54, −11.68, −10.71, −8.58, −7.25, −5.40, −2.74, −0.088, 7.34, 8.49, 13.45, 19.73, 25.66, 28.84, 32.20, 39.19, 46.01 ppm, ^{19}F{^{1}H} NMR (282 MHz, D_2O, 38 °C): δ=−59.43, −59.68 ppm; ^{31}P{^{1}H} NMR (122 MHz, $CDCl_3$, 25 °C): δ=−75.22, 6.33 ppm; ESI-MS (neg.): *m*/*z*: 776.8 $[M-H]^-$. **GdL^1**: ^{19}F{^{1}H} NMR (282 MHz, D_2O, 38 °C): δ=−62.27, −62.53 ppm; ESI-MS (neg.): *m*/*z*: 782.1 $[M-H]^-$; r_1 7.12 mM^{-1}s^{-1} (pH 7.4, MOPS, 300 MHz). **TbL^1**: ^{19}F{^{1}H} NMR (282 MHz, $CDCl_3$, 25 °C): δ=−62.73 ppm; ESI-MS (neg.): *m*/*z*: 783.1 $[M-H]^-$. **YbL^1**: ^{19}F{^{1}H} NMR (282 MHz, $CDCl_3$, 25 °C): δ=−60.03, −60.08, −63.11 ppm; ESI-MS (neg.): *m*/*z*: 797.8 $[M-H]^-$.

Diethyl 4-(trifluoromethyl) phenyl phosphate (2b): 4-(Trifluoromethyl)-phenol **1b** (5.00 g, 30.8 mmol) was dissolved in carbon tetrachloride (30 mL) and this was cooled to 0 °C, triethylamine (5.37 mL, 38.6 mmol) and diethyl phosphite (4.93 mL, 38.6 mmol) were added. After warming the solution to room temperature a white precipitate formed and this was left to stir at this temperature overnight. Water was added followed by dichloromethane and the organic phase was washed with 1 M HCl, saturated sodium chloride solution, dried over sodium sulphate and the solvent was removed under reduced pressure. The crude product was purified using column chromatography (silica gel, from 9:1 to 1:9 hexane/ethyl acetate). Removal of the solvent yielded **2b** as a light yellow oil (8.09 g, 88%). Tlc: R_f=0.47 (silica, hexane/ethyl acetate=7:3); ^{1}H NMR (300 MHz, $CDCl_3$): δ=1.35 (td, $J_{H,H}$=7.2, 0.9 Hz, 6H; OCH_2CH_3); 4.17–4.27 (m, 4H; OCH_2CH_3), 7.33 (dd, $J_{H,H}$=8.9 Hz, 2H; Ar*H*), 7.60 ppm (dd, $J_{H,H}$=8.7 Hz, 2H; Ar*H*); ^{13}C{^{1}H} NMR (75 MHz, $CDCl_3$): δ=15.87 (d, $J_{C,P}$=6.6 Hz; OCH_2CH_3), 64.76 (d, $J_{C,P}$=6.1 Hz; OCH_2CH_3), 120.2 (Ar*C*H), 121.95 (Ar*C*H), 125.55 (Ar*C*), 126.97 (q, $J_{C,F}$=3.9 Hz; CCF_3), 153.21 ppm(Ar*C*); ^{19}F{^{1}H} NMR (282 MHz, $CDCl_3$,): δ=−62.24 ppm; ^{31}P{^{1}H} NMR (122 MHz, $CDCl_3$): δ=−6.77 ppm; ESI-MS (pos.): *m*/*z*: 299 $[M+H]^+$, 321 $[M+Na]^+$, 337 $[M+K]^+$; HRMS (EI): *m*/*z*: calcd for $C_{11}H_{14}O_4F_3P_1$: 298.05818; found: 298.06124.

Diethyl 2-hydroxy-5-(trifluoromethyl) phenylphosphonate (3b): A flask containing the phosphate ester **2b** (8.00 g, 26.80 mmol) was purged of air and kept under dinitrogen, dry tetrahydrofuran (30 mL was added and the solution was cooled to −78 °C. A solution of lithium diisopropylamine also under a dinitrogen atmosphere, was prepared over 30 min by dissolving diisopropylamine (11.36 mL, 80.40 mmol) in tetrahyrofuran (20 mL) and cooling this to −78 °C, followed by the addition of *n*-butyl lithium (50.25 mL, 1.6 M, 80.4 mmol). This was then transferred via cannula to the phosphate solution, which changed the solution to a caramel color. After 3 h saturated ammonium solution was added to quench the reaction and the solution was warmed to room temperature. The product was extracted into diethyl ether; the organic phase was washed with saturated sodium chloride solution and dried over sodium sulphate. The solvent was removed under reduced pressure and the crude product was purified using column chromatography (silica gel, from 9:1 to 3:7 hexane/ethyl acetate). On removal of the solvent **3b** was isolated as an orange oil (5.71 g, 71%). Tlc: R_f=0.50 (silica, EtOAc/hexane=3:7); ^{1}H NMR (300 MHz, $CDCl_3$,): δ=1.27 (t, 6H, $^3J_{H,H}$=7.2 Hz; $POCH_2CH_3$), 3.94–4.18 (m, 4H; $POCH_2CH_3$), 6.94–6.99 (m 1H; Ar*H*), 7.53–7.59 (m, 2H; Ar*H*), 10.59 ppm (s, 1H; PhO*H*); ^{13}C{^{1}H} NMR (75 MHz, $CDCl_3$,): δ=16.04 (d, $J_{C,P}$=6.6 Hz; OCH_2CH_3), 63.13 (d, $J_{C,P}$=5.0 Hz; OCH_2CH_3), 108.35 (Ar*C*H), 110.77 (Ar*C*H), 118.26 (Ar*C*H), 121.98 (Ar*C*), 129.15 (CCF_3), 131.81 (Ar*C*), 164.50 ppm (Ar*C*); ^{19}F{^{1}H} NMR (282 MHz, $CDCl_3$): δ=−61.93 ppm; ^{31}P{^{1}H} NMR (122 MHz, $CDCl_3$): δ=20.18 ppm; ESI-MS (pos.): *m*/*z*: 299 $[M+H]^+$, 321 $[M+Na]^+$, 337 $[M+K]^+$, (neg.): *m*/*z*: 297 $[M-H]^-$. HRMS (EI): *m*/*z*: calcd for $C_{11}H_{14}O_4F_3P_1$: 298.05818; found: 298.05822.

Diethyl 2-(3-bromopropoxy)-5-(trifluoromethyl) phenylphosphonate (4b): The phenol **3b** (2.0 g, 6.71 mmol) was dissolved in anhydrous dimethylformamide (20 mL) and potassium carbonate (1.85 g, 13.41 mmol) was added, this was heated to 60 °C for 1 hour under a dinitrogen atmosphere, changing the solution to a brown color. Dibromopropane (2.05 mL, 20.19 mmol) was added dropwise and the mixture was heated for a further 17 h. After cooling to room temperature the inorganic salts were removed by filtration and dichloromethane was added. The organic phase was washed with saturated sodium chloride solution, dried over sodium sulphate and the solvent was removed under reduced pressure. The crude product was purified using column chromatography (silica gel, from 9:1 hexane/ethyl acetate to 100% ethyl acetate). Removal of the solvents yielded **4b** as a light yellow oil (1.82 g, 65%). Tlc: R_f=0.29 (silica, EtOAc/hexane=1:1); ^{1}H NMR (300 MHz, $CDCl_3$): δ=1.33 (t, 6H, $^3J_{H,H}$=7.0 Hz; $POCH_2CH_3$), 2.36 (quin, 2H, $^3J_{H,H}$=5.9 Hz; $BrCH_2CH_2$); 3.73 (t, 2H, $^3J_{H,H}$=6.2 Hz; $BrCH_2CH_2CH_2$), 4.04–4.27 (m, 6H, $POCH_2CH_3$; $BrCH_2$), 7.00–7.05 (m, 1H; Ar*H*), 7.76 (d, 1H, $^3J_{H,H}$=8.7 Hz; Ar*H*), 8.12 ppm (d, 1H, J=15.3 Hz; Ar*H*); ^{13}C{^{1}H} NMR (75 MHz, $CDCl_3$): δ=16.14, 29.52, 31.69, 62.14, 65.71, 69.18, 111.70, 112.11, 117.97, 118.61, 122.44, 125.50, 131.39, 132.45, 162.38 ppm; ^{19}F{^{1}H} NMR (282 MHz, $CDCl_3$): δ=−61.78 ppm; ^{31}P{^{1}H} NMR (122 MHz, $CDCl_3$); δ=14.46, 14.85 ppm; ESI-MS (pos.): *m*/*z*: 420 $[M+H]^+$, 442 $[M+Na]^+$; HRMS (EI): *m*/*z*: for $C_{14}H_{20}O_4F_3P_1Br_1$: 420.013596; found: 420.01622.

Tri-*tert*-butyl 2,2′,2″-(10-(3-(2-(diethoxyphosphoryl)-4-(trifluoromethyl)-phenoxy)propyl)-1,4,7,10-tetraazacyclododecane-1,4,7-triyl)triacetate (5b): Tris *tert*-butyl-DO3A (1.51 g, 2.54 mmol), the phosphonate arm **4b** (1.62 g, 3.86 mmol) and potassium carbonate (1.05 g, 7.61 mmol) were dissolved in acetonitrile (20 mL) and the mixture was heated to 70 °C

under a dinitrogen atmosphere. After 48 h the solution was cooled to room temperature, the inorganic salts were removed by filtration and the solvent was evaporated under reduced pressure. The resulting yellow oil was dissolved in dichloromethane and washed with saturated sodium chloride solution, dried over sodium sulphate and the solvent evaporated. The crude product was purified using column chromatography (alumina from 100% dichloromethane to 96:4 dichloromethane/methanol). On removal of the solvents **5b** was isolated as a yellow solid (1.89 g, 87%). Tlc: R_f=0.33 (alumina, dichloromethane/methanol=92.5:7.5); ^{1}H NMR (300 MHz, $CDCl_3$): δ=1.30 (t, 6H, $^3J_{HH}$=7.0 Hz; $POCH_2CH_3$), 1.40–1.42 (m, 27H; CCH_3), 1.99–4.30 (br m, 34H; CH_2 ring, NCH_2COO, $NCH_2CH_2CH_2O$, $POCH_2CH_3$), 7.12–7.17 (m, 1H; Ar*H*), 7.72–7.74 (m, 1H; Ar*H*), 8.00 ppm (d, 1H, J=15.11 Hz; Ar*H*); ^{13}C{^{1}H} NMR (75 MHz, $CDCl_3$): δ=16.11, 24.75, 27.55, 49.62, 50.23, 51.79, 55.35, 61.89, 67.06, 80.29, 82.32, 111.92, 115.79, 118.29, 121.98, 131.25, 132.25, 162.42, 170.62, 172.30, 173.37 ppm; ^{19}F{^{1}H} NMR (282 MHz, $CDCl_3$): δ=−61.77, −61.65 ppm; ^{31}P{^{1}H} NMR (122 MHz, $CDCl_3$): δ=14.54, 15.05 ppm; ESI-MS (pos.): m/z: 853.5 $[M+H]^+$; HRMS (FT-ICR): m/z: calcd for $C_{40}H_{69}F_3N_4O_{10}P_1$: 853.46979 $[M+H]^+$; found: 853.46965.

2,2′,2″-(10-(3-(2-Phosphono-4-(trifluoromethyl)phenoxy)propyl)-1,4,7,10-tetraazacyclododecane-1,4,7-triyl)triacetic acid (L^2): The ester **5b** (0.948 g, 1.11 mmol) was dissolved in dimethylformamide (5 mL), this was cooled to 0°C in an ice bath and bromotrimethylsilane (0.733 mL, 5.56 mmol) was added dropwise to the solution. This was warmed to room temperature and stirred for 18 h. The solvent was evaporated under reduced pressure and the removal of the ethyl groups was confirmed through electrospray mass spectrometry. A mixture of dichloromethane and trifluoroacetic acid (1:1, 10 mL) was added to the crude orange oil and the mixture was stirred at room temperature for 48 h. Following removal of the solvents a brown oil was obtained and electrospray mass spectrometry again confirmed the removal of the *tert*-butyl groups. The crude product was purified through reverse phase HPLC. On freeze drying the $\mathbf{L^2}$ was isolated as a flocculent white solid that quickly became a yellow oil due to its hygroscopic nature (0.664 g, 95%). ^{1}H NMR (300 MHz, D_2O): δ=2.21–4.12 (br m, 28H; CH_2 ring, NCH_2COO, $NCH_2CH_2CH_2O$,), 7.03–7.87 ppm (m, 3H; Ar*H*); ^{13}C{^{1}H} NMR (75 MHz, D_2O): δ=22.69, 31.31, 36.80, 48.42, 49.79, 51.41, 53.31, 56.03, 65.23, 110.57, 111.89, 114.44, 118.32, 118.87, 121.75, 122.43, 124.45, 126.02, 129.84, 161.78, 162.27, 162.74, 164.74, 169.64, 172.99, 174.48, 174.45 ppm; ^{19}F{^{1}H} NMR (282 MHz, D_2O): δ=−61.18 ppm; ^{31}P{^{1}H} NMR (122 MHz, D_2O): δ=8.78 ppm, ESI-MS (pos.): m/z: 629.3 $[M+H]^+$, 657.3 $[M+Na]^+$; HRMS (FT-ICR): m/z: calcd for $C_{24}H_{35}F_3N_4O_{10}P_1$: 627.20484 $[M-H]^-$; found: 627.20466.

2,2′,2″-(10-(3-(2-Phosphono-4-(trifluoromethyl)phenoxy)propyl)-1,4,7,10-tetraazacyclododecane-1,4,7-triyl)triacetic acid lanthanide complex (LnL^2)

EuL^2: ^{1}H NMR (300 MHz, D_2O): δ=−20.88, −19.15, −17.51, −16.26, −14.15, −12.13, −10.97, −7.99, −6.16, −3.66, −2.41, −1.44, 0.86, 1.35, 1.83, 2.89, 3.56, 6.83, 10.39, 13.28, 20.79, 26.85, 28.49, 30.60, 42.34 ppm; ^{19}F{^{1}H} NMR (282 MHz, D_2O, 38°C): δ=−64.15 ppm; ^{31}P{^{1}H} NMR (122 MHz, $CDCl_3$, 25°C): δ=−130.02, 9.28 ppm; ESI-MS (neg.): m/z: 776.8 $[M-H]^-$. **GdL^2**: ^{19}F{^{1}H} NMR (282 MHz, D_2O, 38°C): δ=−62.27, −62.53 ppm; ESI-MS (neg.): m/z: 782.0 $[M-H]^-$; r_1 6.64 mM^{-1}s^{-1} (pH 7.4, MOPS, 300 MHz). **TbL^2**: ^{19}F{^{1}H} NMR (282 MHz, $CDCl_3$, 25°C): δ=−62.73 ppm; ESI-MS (neg.): m/z: 783.0 $[M-H]^-$. **YbL^2**: ^{19}F{^{1}H} NMR (282 MHz, $CDCl_3$, 25°C): δ=−60.65, −76.63 ppm; ESI-MS (neg.): m/z: 797.8 $[M-H]^-$.

Diethyl (2-((4-(bromomethyl) benzyl) oxy)-3-(trifluoromethyl) phenyl) phosphonate (4c): The phenol **3a** (3.70 g, 12.41 mmol) was dissolved in anhydrous dimethylformamide (100 mL) and potassium carbonate was added (3.43 g, 24.82 mmol) and this was heated to 60°C under a dinitrogen atmosphere. After 1 hour this was added dropwise to a solution of 1,4-bis (bromomethyl) benzene (32.8 g, 124 mmol) in dimethylformamide (50 mL) and the mixture was heated for 18 h. The solvent was removed under reduced pressure, and diethyl ether was added precipitating most of the bromide starting material from solution which was removed by filtration. Evaporation of diethyl ether yielded an orange solid which was purified using column chromatography (silica gel, from 9:1 hexane/ethyl acetate to 100% ethyl acetate). Removal of the solvent yielded **4c** as a yellow oil. (4.05 g, 68%). Tlc: R_f=0.35 (silica, EtOAc/hexane 1:1); ^{1}H NMR (300 MHz, $CDCl_3$): δ=1.30 (t, 6H, $^3J_{H,H}$=7.0 Hz; $POCH_2CH_3$), 4.09–4.22 (m, 4H; $POCH_2CH_3$), 4.52 (s, 2H; CCH_2O), 5.25 (s, 2H; CCH_2Br), 7.30–7.44 (m, 3H; Ar*H*), 7.58 (d, 1H, $^3J_{H,H}$=8.31 Hz; Ar*H*), 7.85 (d, 1H, $^3J_{H,H}$=7.00 Hz; Ar*H*), 8.03–8.16 ppm (m, 1H; Ar*H*); ^{13}C{^{1}H} NMR (75 MHz, $CDCl_3$): δ=16.23, 33.27, 62.66, 121.47, 124.23, 125.63, 127.29, 128.84, 131.80, 137.03, 137.50, 138.53, 159.16, 160.71 ppm; ^{19}F{^{1}H} NMR (282 MHz, $CDCl_3$): δ=−60.12, −60.10 ppm; ^{31}P{^{1}H} NMR (122 MHz, $CDCl_3$): δ=14.01, 16.02 ppm; ESI-MS (pos.): m/z: 482 $[M+H]^+$; HRMS (EI): m/z: calcd for $C_{19}H_{21}O_4F_3P_1Br_1$: 482.029246; found: 482.02574.

Tri-*tert*-butyl 2,2′,2″-(10-(4-((2-(diethoxyphosphoryl)-6-(trifluoromethyl)-phenoxy)methyl)benzyl)-1,4,7,10-tetraazacyclododecane-1,4,7-triyl)triacetate (5c): Tris *tert*-butyl-DO3A (3.98 g, 6.69 mmol), 4c (4.0 g, 8.36 mmol) and potassium carbonate (2.77 g, 20.06 mmol) were added to dimethylformamide (20 mL) and the mixture was heated to 60°C under a dinitrogen atmosphere for 48 h. The solvent was removed under reduced pressure, and dichloromethane was added. Following the removal of the inorganic salts the organic phase was washed with saturated sodium chloride solution and dried over sodium sulphate. Removal of the solvent yielded an orange oil. The crude product was purified using column chromatography (alumina from 100% dichloromethane to 93:7 dichloromethane/methanol). Removal of the solvents yielded **5c** as a yellow solid (4.77 g, 78%). Tlc: R_f=0.25 (alumina, dichloromethane/methanol=95:5); ^{1}H NMR (300 MHz, $CDCl_3$); δ=1.20–1.40 (m, 33H; $POCH_2CH_3$, CCH_3), 2.16–4.10 (br m, 34H; CH_2 ring, NCH_2COO, $NCH_2CH_2CH_2O$, $POCH_2CH_3$), 5.16 (s, 2H; CCH_2N), 7.25–7.50 (m, 5H; Ar*H*), 7.76–7.79 (m, 1H; Ar*H*), 7.97–8.02 ppm (m, 1H; Ar*H*); ^{13}C{^{1}H} NMR (75 MHz, $CDCl_3$): δ=14.90, 15.96, 27.57, 49.64, 51.18, 55.33, 33.66, 59.19, 62.29, 65.42, 80.26, 82.04, 82.50, 126.57, 126.86, 128.00, 128.26, 129.63, 131.49, 135.90, 136.84, 138.25, 158.74, 170.72, 172.16, 173.16 ppm; ^{19}F{^{1}H} NMR (282 MHz, $CDCl_3$): δ=−60.19, −60.16, −60.11, −60.02 ppm; ^{31}P{^{1}H} NMR (122 MHz, $CDCl_3$): δ=13.92, 14.20 ppm; ESI-MS (pos.): m/z: 915.5 $[M+H]^+$, 937.5 $[M+Na]^+$; HRMS (FT-ICR): m/z: calcd for $C_{45}H_{71}F_3N_4O_{10}P_1$: 915.48544 $[M+H]^+$; found: 915.48555.

2,2′,2″-(10-(4-((2-Phosphono-6-(trifluoromethyl)phenoxy)methyl)benzyl)-1,4,7,10-tetraazacyclododecane-1,4,7-triyl)triacetic acid (L^3): The ester **5c** (1.0 g, 1.09 mmol) was dissolved in dimethylformamide (5 mL) and cooled to 0°C in an ice bath, bromotrimethylsilane (0.72 mL, 5.46 mmol) was added slowly and the solution was stirred at room temperature for 18 h. The absence of the ethyl esters was confirmed by electrospray mass spectrometry. A mixture of dichloromethane and trifluoroacetic acid (1:1, 10 mL) was added to the crude orange oil and the mixture was stirred at room temperature for 48 h. Following removal of the solvents a brown oil was obtained and electrospray mass spectrometry again confirmed the removal of the *tert*-butyl groups. The crude product was purified through reverse phase HPLC. On freeze drying $\mathbf{L^3}$ was isolated as a flocculent white solid that quickly became a yellow oil due to its hygroscopic nature (0.661 g, 88%).^{1}H NMR (300 MHz, D_2O): δ=2.75–3.85 (br m, 28H; CH_2 ring, NCH_2COO, $NCH_2CH_2CH_2O$,), 7.07–7.88 (m, 3H; Ar*H*) ppm; ^{13}C{^{1}H} NMR (75 MHz, D_2O): δ=29.57, 48.18, 49.40, 54.66, 56.88, 77.15, 121.86, 124.30, 125.47, 129.37, 130.83, 133.12, 138.13, 157.43, 172.05 ppm; ^{19}F{^{1}H} NMR (282 MHz, D_2O): δ=−62.23, −59.91 ppm; ^{31}P{^{1}H} NMR (122 MHz, D_2O): δ=7.36, 12.10 ppm; ESI-MS (neg.): m/z: 689.1 $[M-H]^-$; HRMS (FT-ICR): m/z: calcd for $C_{29}H_{37}F_3N_4O_{10}P_1$: 689.22049 $[M-H]^-$; found: 689.22093.

2,2′,2″-(10-(4-((2-Phosphono-6-(trifluoromethyl)phenoxy)methyl)benzyl)-1,4,7,10-tetraazacyclododecane-1,4,7-triyl)triacetic acid lanthanide complex (LnL^3)

YL^3: ESI-MS (neg.): m/z: 774.9 $[M-H]^-$. **EuL^3** ^{1}H NMR (300 MHz, D_2O, 25°C): δ=−25.24, −21.68, −19.67, −18.74, −14.00, −13.53, −13.09, −12.22, −11.74, −7.56, −4.90, −3.51, −2.09, 1.13, 3.29, 6.91, 7.52, 8.14, 9.22, 12.83, 14.93, 26.45, 30.99, 47.50 ppm; ^{19}F{^{1}H} NMR (282 MHz, D_2O, 25°C): δ=−64.83, −63.81 ppm; ^{31}P{^{1}H} NMR (122 MHz, $CDCl_3$, 25°C): δ=−118.42, 13.59 ppm; ESI-MS (neg.): m/z: 838.8 $[M-H]^-$. **GdL^3**: ^{19}F{^{1}H} NMR (282 MHz, D_2O, 25°C): δ=−64.38, −64.27 ppm; ESI-MS (neg.): m/z: 844.1 $[M-H]^-$, 866.1 $[M-2H+Na]^-$; r_1 6.12 mM^{-1}s^{-1} (pH 7.4,

MOPS, 300 MHz). **TbL^3**: ^{19}F{^{1}H} NMR (282 MHz, D_2O, 25 °C): $\delta = -62.25$ ppm; ESI-MS (neg.): m/z: 845.1 $[M-H]^-$. **YbL^3**: ^{19}F{^{1}H} NMR (282 MHz, D_2O, 25 °C): $\delta = -55.69, -58.63, -61.60$ ppm; ESI-MS (neg.): m/z: 859.8 $[M-H]^-$.

Diethyl (2-((4-(bromomethyl) benzyl) oxy)-5-(trifluoromethyl) phenyl) phosphonate (4d): The phenol **3b** (2.80 g, 9.39 mmol) was dissolved in anhydrous dimethylformamide (100 mL) and potassium carbonate was added (2.60 g, 18.78 mmol) and this was heated to 60 °C under a dinitrogen atmosphere. After 1 hour this was added dropwise to a solution of 1,4-bis (bromomethyl) benzene (24.79 g, 93.92 mmol) in dimethylformamide (50 mL) and the mixture was heated for 18 h. The solvent was removed under reduced pressure, and diethyl ether was added precipitating most of the bromide starting material from solution which was removed by filtration. Evaporation of diethyl ether yielded an orange solid which was purified using column chromatography (silica gel, from 9:1 hexane/ethyl acetate to 100 % ethyl acetate). Removal of the solvent yielded **4d** as a white solid. (3.37 g, 75 %). Tlc: $R_f = 0.42$ (silica, EtOAc/hexane = 1:1); ^{1}H NMR (300 MHz, $CDCl_3$); $\delta = 1.28$ (t, 6H, $^3J_{H,H} = 7.2$ Hz; $POCH_2CH_3$), 4.02–4.23(m, 4H; $POCH_2CH_3$), 4.48 (s, 2H; CCH_2O), 5.22 (s, 2H; CCH_2Br), 7.00–7.05 (m, 1H; Ar*H*), 7.41 (d, 1H, $^3J_{H,H} = 8.3$ Hz; Ar*H*), 7.48 (d, 1H, $^3J_{H,H} = 8.3$ Hz; Ar*H*), 7.70 (d, 1H, $^3J_{H,H} = 8.7$ Hz; Ar*H*), 8.12 ppm (d, 1H, $^3J_{H,H} = 15.3$ Hz; Ar*H*), ^{13}C{^{1}H} NMR (75 MHz, $CDCl_3$): $\delta = 16.22$, 32.86, 62.38, 70.00, 112.26, 116.92, 119.43, 121.98, 122.60, 123.05, 123.24, 127.30, 129.21, 131.27, 132.43, 135.80, 137.69, 162.22 ppm; ^{19}F{^{1}H} NMR (282 MHz, $CDCl_3$) $\delta = -61.72$ ppm; ^{31}P{^{1}H} NMR (122 MHz, $CDCl_3$): $\delta = 14.47$ ppm; ESI-MS (pos.): m/z: 482 $[M+H]^+$; HRMS (EI): m/z: calcd for $C_{19}H_{21}O_4F_3P_1Br_1$: 482.029246; found: 482.02514.

Tri-*tert*-butyl 2,2′,2″-(10-(4-((2-(diethoxyphosphoryl)-4-(trifluoromethyl)-phenoxy)methyl)benzyl)-1,4,7,10-tetraazacyclododecane-1,4,7-triyl)triacetate (5d): Tris *tert*-butyl-DO3A (2.20 g, 3.69 mmol), 4d (2.67 g, 5.54 mmol) and potassium carbonate (1.53 g, 11.08 mmol) were added to dimethylformamide (20 mL) and the mixture was heated to 60 °C under a dinitrogen atmosphere for 48 h. The solvent was removed under reduced pressure, and dichloromethane was added. Following the removal of the inorganic salts the organic phase was washed with saturated sodium chloride solution and dried over sodium sulphate. Removal of the solvent yielded an orange oil. The crude product was purified using column chromatography (alumina from 100 % dichloromethane to 93:7 dichloromethane/methanol). Removal of the solvents yielded **5d** as a yellow solid (1.91 g, 91 %). Tlc: $R_f = 0.25$ (alumina, dichloromethane/methanol = 95:5); ^{1}H NMR (300 MHz, $CDCl_3$): $\delta = 1.18$–1.39 (m, 33H, $POCH_2CH_3$; CCH_3), 1.97–4.14 (br m, 34H; CH_2 ring, NCH_2COO, $NCH_2CH_2CH_2O$, $POCH_2CH_3$), 5.17 (s, 2H; CCH_2Br), 6.98–7.04 (m, 1H; Ar*H*), 7.27–7.44 (m, 4H; Ar*H*), 7.66 (t, 1H, $^3J_{H,H} = 7.18$ Hz; Ar*H*), 8.05 ppm (d, 1H, $^3J_{H,H} = 15.30$ Hz; Ar*H*); ^{13}C{^{1}H} NMR (75 MHz, $CDCl_3$): $\delta = 16.13$, 27.78, 29.44, 49.46, 51.71, 51.91, 51.97, 55.57, 55.91, 56.32, 58.86, 59.62, 62.22, 69.98, 70.36, 80.39, 82.23, 82.64, 112.35, 116.63, 119.94, 122.23, 126.81, 129.06, 130.26, 131.21, 134.97, 136.84, 139.81, 162.25, 171.00, 172.38, 173.34 ppm; ^{19}F{^{1}H} NMR (282 MHz, $CDCl_3$): $\delta = -61.72, -61.69$ ppm; ^{31}P{^{1}H} NMR (122 MHz, $CDCl_3$): $\delta = 14.57$ ppm; ESI-MS (pos.): m/z: 915.5 $[M+H]^+$, 937.5 $[M+Na]^+$; HRMS (FT-ICR): m/z: calcd for $C_{45}H_{71}F_3N_4O_{10}P_1$: 915.48544 $[M+H]^+$; found: 915.48533.

2,2′,2″-(10-(4-((2-Phosphono-4-(trifluoromethyl)phenoxy)methyl)benzyl)-1,4,7,10-tetraazacyclododecane-1,4,7-triyl)triacetic acid (L^4): The ester **5d** (0.427 g, 0.467 mmol) was dissolved in dimethylformamide (5 mL) and cooled to 0 °C in an ice bath, bromotrimethylsilane (0.647 mL, 4.91 mmol) was added slowly and the solution was stirred at room temperature for 18 h. The absence of the ethyl esters was confirmed by electrospray mass spectrometry. A mixture of dichloromethane and trifluoroacetic acid (1:1, 10 mL) was added to the crude orange oil and the mixture was stirred at room temperature for 24 h. Following removal of the solvents a brown oil was obtained and electrospray mass spectrometry again confirmed the removal of the *tert*-butyl groups. The crude product was purified through reverse phase HPLC. On freeze drying **L^4** was isolated as a flocculent white solid that quickly became a yellow oil due to its hygroscopic nature (0.253 g, 79 %). ^{1}H NMR (300 MHz, D_2O): $\delta = 2.96$–4.16 (br m, 28H; CH_2 ring, NCH_2COO, $NCH_2CH_2CH_2O$,), 5.25 (s, 2H, CCH_2N), 7.07 (t, $^3J_{H,H} = 6.23$ Hz, 1H; Ar*H*), 7.43–7.51 (m, 4H; Ar*H*), 7.67 (d, $^3J_{H,H} = 7.9$ Hz, 1H; Ar*H*), 7.96 ppm (d, $^3J_{H,H} = 14.5$ Hz, 1H; Ar*H*); ^{13}C{^{1}H} NMR (75 MHz, D_2O): $\delta = 28.72$, 28.79, 51.15, 53.36, 54.98, 56.37, 58.64, 71.14, 83.59, 85.79, 114.70, 114.82, 120.56, 123.09, 123.69, 123.90, 127.28, 129.19, 131.93, 132.51, 133.00, 139.92, 163.78, 166.77, 172.52 ppm; ^{19}F{^{1}H} NMR (282 MHz, D_2O): $\delta = -61.24$ ppm; ^{31}P{^{1}H} NMR (122 MHz, D_2O): $\delta = 8.61$ ppm; ESI-MS (neg.): m/z: 689.1 $[M-H]^-$; HRMS (FT-ICR): m/z calcd for $C_{29}H_{37}F_3N_4O_{10}P_1$: 689.22049 $[M-H]^-$; found: 689.22028.

2,2′,2″-(10-(4-((2-Phosphono-4-(trifluoromethyl)phenoxy)methyl)benzyl)-1,4,7,10-tetraazacyclododecane-1,4,7-triyl)triacetic acid lanthanide complex (LnL^4)

EuL^4: ^{1}H NMR (300 MHz, D_2O): $\delta = -20.91, -18.48, -14.40, -12.06, -10.38, -9.81, -8.58, -7.63, -4.55, -3.89, -2.48, -0.08$, 1.25, 7.33, 9.73, 10.56, 15.22, 27.07, 21.93, 24.93, 26.15, 27.65, 31.58, 33.56, 37.31, 39.63, 42.20, 48.05 ppm; ^{19}F{^{1}H} NMR (282 MHz, D_2O, 25 °C): $\delta = -60.71, -61.08$ ppm; ^{31}P{^{1}H} NMR (122 MHz, $CDCl_3$, 25 °C): $\delta = -139.50, -112.34$, 11.93 ppm; ESI-MS (neg.): m/z: 838.8 $[M-H]^-$. **GdL^4**: ^{19}F{^{1}H} NMR (282 MHz, D_2O, 25 °C): $\delta = -60.45$ ppm; ESI-MS (neg.): m/z: 844.1 $[M-H]^-$; r_1 6.12 mM^{-1}s^{-1} (pH 7.4, MOPS, 300 MHz). **TbL^4**: ^{19}F{^{1}H} NMR (282 MHz, D_2O, 25 °C) $-60.98, -63.15$ ppm; ESI-MS (neg.): m/z: 845.2 $[M-H]^-$. **YbL^4**: ^{19}F{^{1}H} NMR (282 MHz, D_2O, 25 °C): $\delta = -60.54$ ppm; ESI-MS (neg.): m/z: 859.8 $[M-H]^-$.

NMR spectroscopy and mass spectrometry: ^{1}H, ^{13}C {^{1}H}, ^{31}P {^{1}H} and ^{19}F {^{1}H} NMR spectra, ^{1}H and ^{19}F T_1 and T_2 times were recorded on a Bruker Avance III 300 MHz 'Microbay' spectrometer at 25 °C Bruker (Germany). ^{19}F T_1 and T_2 times were measured using inversion recovery and Carr-Purcell-Meiboom-Gill sequences respectively, on 5 mM solution of complex in MOPS buffer (0.1 M, pH 7.4). The exact concentrations of the complexes were determined by measurement of bulk magnetic susceptibility shifts of a *t*BuOH signal.[54] Variable pH relaxivities were determined through inversion recovery measurements, where the pH was adjusted using solid LiOH or TsOH to minimize the change in concentration. Variable-temperature ^{17}O NMR measurements were recorded on a Bruker Avance III (11.7 T) spectrometer equipped with a 5 mm probe and standard temperature control units. Aqueous solutions of the complexes (5–20 mM) containing 2.0 % of the ^{17}O isotope (Cambridge Isotope) were used. The observed transverse relaxation rates were calculated from the signal width at half-height. ^{1}H DOSY measurements were carried out nonspinning on a Varian VNMRS 500 MHz spectrometer at 296 K using the Oneshot DOSY pulse sequence. Data were acquired with an array of 16 gradient amplitudes ranging from 3.0 G cm^{-1} to 27.0 G cm^{-1} in equal steps of gradient squared, using 16 transients, 65536 complex data points, a total diffusion encoding gradient of 2 ms and a diffusion time of 0.05 s. DOSY spectra were constructed using correction for the effects of pulsed field gradient nonuniformity. ESI-LRMS were performed on an ion trap SL 1100 system Agilent (Germany). FT-ICR-MS were performed on a Bruker FT-ICR Apex II spectrometer Agilent (Germany). HR-EI-MS were performed on a MAT Sektorfeld mass spectrometer Finnigan (Germany).

Luminescence spectroscopy: Steady-state and time resolved measurements were performed on a QuantaMasterTM 3 PH fluorescence spectrometer from Photon Technology International, Inc. (USA). Details regarding the luminescence measurements for **TbL$^{5-8}$** are given in the supplementary information of the previous work.[16] The steady state measurements were performed in H_2O (25 °C, pH 7.4, MOPS) at a concentration of 250 μM for **EuL$^{1-4}$**, 50 μM for **TbL$^{1-4}$**, and 5 mM for **EuL$^{5-8}$**. Excitation and emission slits were set to 2 nm for **EuL$^{1-8}$** and **TbL$^{1-4}$**, datasets are an average of 10 scans. The time resolved measurements were performed in H_2O and D_2O (25 °C, pH 7.4, MOPS) at a concentration of 50 μM for **TbL$^{1-4}$** and 5 mM for **EuL$^{1-8}$**. Excitation and emission slits were set to 15 and 5 nm band pass respectively, with 10 μs resolution. Datasets are recorded with a 100 μs delay and are an average of 15 scans. Each reported value is the mean of three independent measurements and obtained curves are fitted to the first order exponential decay with $R^2 > 0.99$.

Relaxometry: The proton $1/T_1$ NMRD profiles were measured on a fast field-cycling Stelar SmartTracer relaxometer over a continuum of mag-

netic field strengths from 0.00024 to 0.25 T (corresponding to 0.01–10 MHz proton Larmor frequencies). The relaxometer operates under computer control with an absolute uncertainty in $1/T_1$ of ±1%. Additional data points in the range 15–70 and 500 MHz were obtained on a Bruker WP80 NMR electromagnet adapted to variable-field measurements (15–80 MHz proton Larmor frequency) Stelar Relaxometer and Bruker Avance III 500 MHz (11.7 T) spectrometer respectively. The ^1H T_1 relaxation times were acquired by the standard inversion recovery method with typical 90° pulse width of 3.5 μs, 16 experiments of 4 scans. The reproducibility of the T_1 data was ±5%. The temperature was controlled with a Stelar VTC-91 airflow heater equipped with a calibrated copper-constantan thermocouple (uncertainty of ±0.1 °C).

Equilibrium measurements: The chemicals used in the equilibrium measurement experiments were of the highest analytical grade. For the preparation of the $LnCl_3$ solutions, Ln_2O_3 (Fluka, 99.9%) was dissolved in 6.0 M HCl and the excess acid was evaporated. The concentration of the $LnCl_3$, $CaCl_2$, $CuCl_2$, and $ZnCl_2$ solutions were determined by complexometric titration with standardized Na_2H_2EDTA and xylenol orange ($LnCl_3$), murexide ($CuCl_2$, $ZnCl_2$), and Patton & Reeder ($CaCl_2$) as indicators. The concentration and the protonation constants of **L**[1,3,8] were determined by pH-potentiometric titrations in the presence and absence of a large (40-fold) excess of $CaCl_2$. All the equilibrium measurements were carried out at constant 0.15 M NaCl ionic strength at 25 °C. The protonation and stability constants of the Ca^{2+}, Zn^{2+}, Cu^{2+}, and Gd^{3+} complexes of **L**[1,3,8], **CaDOTA**, **ZnDOTA**, as well as the stability constants of the intermediate complexes, ***GdH$_3$L**[1] and ***GdH$_4$L**[8] were also determined by means of pH-potentiometric titration. The stability constants for Ca^{2+} and Zn^{2+} complexes of DOTA are lower from those previously reported due to the lower first protonation constant related to the formation of the relatively stable NaDOTA complex.[55] The protonation constants of the Gd^{3+} complexes were determined in the pH range 3–12 avoiding their dissociation at pH < 3,0. The best fitting was obtained by using the model which includes the formation of ML and $MH_{1-5}L$ species in equilibrium depending on the investigated system. In all cases the metal-to-ligand concentration ratios were 1:1. The concentration of the ligands was generally 2–3 mM. For the calculation of the protonation and stability constants mL base–pH data pairs (80–100), obtained in the pH range of 1.7–12, were used. Because of the slow formation rates of the macrocyclic Gd^{3+} complexes "out-of-cell" technique was used to determine their stability constants. 8 samples were prepared for the systems Gd-**L**[1,8] at a 2 mM concentration between pH 2–4. After 1 month equilibration time the pH and relaxivity values of the samples were measured. For the calculation of the stability constants of the Gd^{3+} complexes, the protonation constant of the ligands and the complexes as well as the stability constants of the intermediates were also considered. The determination of the stability constants of Cu^{2+} complexes were carried out by following the formation of Cu^{2+} complexes with spectrophotometry in very acidic solutions (c_{H+} = 0.01–1,0 M). The concentration of Cu^{2+} and the ligands in the samples were 1 mM (6 samples were prepared for each system). The total H^+ concentration in the samples was adjusted by the addition of a calculated amount of 3 M HCl. The ionic strength was not constant in these samples. For the equilibrium calculations, the protonation constants of the Cu^{2+} complexes, the molar absorptivities of the $CuCl_2$ and the **CuL**[1,3,8] complexes with different protonation states were used. The molar absorptivities of **CuL**[1,3,8] complexes and those of protonated forms were determined at 11 wavelengths between 575–775 nm by recording the spectra of $1.0–4.0\times10^{-3}$ M solutions of **CuL**[1,3,8] complexes in the pH range 1.5–6.0 (0.15 M NaCl, 25 °C). After 1 month equilibration time, the absorbance values of the samples were measured also at 11 wavelengths, as before. The spectrophotometric measurements were made by using Cary 1E spectrophotometer at 25 °C. The optical length was 10 mm. The pH-potentiometric titrations were carried out with a *Methrohm 785DMP Titrino* titration workstation with the use of a *Metrohm-6.0233.100* combined electrode. The titrated solution (10.00 mL) was thermostated at 25 °C. The samples were stirred and to avoid the effect of CO_2, N_2 gas was bubbled through the solutions. The titrations were made in the pH range 1.7–12. For the calibration of the pH meter, KH-phthalate (pH 4.005) and borax (pH 9.177) buffers were used. The concentrations of the H^+ ions were calculated from the measured pH values using the method proposed by *Irving* et al.[56] A 0.01 M HCl (0.15 M NaCl solution was titrated with 0.2 M NaOH and the difference between the measured and calculated pH values was used to calculate the $[H^+]$ from the pH values determined in the titration experiments. For the calculation of the equilibrium constants the PSEQUAD program was used.[57]

Kinetic measurements: The rates of the metal exchange reactions of the Gd^{3+} complexes of **L**[1,3,8] with Cu^{2+} ion were studied by UV-spectrophotometry, following the formation of the Cu^{2+} complexes at 300 nm with the use of 1.0 cm cells and Cary 1E spectrophotometer. The concentration of the complexes was 1×10^{-4} M, whereas the concentration of the Cu^{2+} was 10-times higher, in order to guarantee the pseudo-first-order conditions. Some reactions were performed by using 40-fold excess of the Cu^{2+} ion to get information on the role of the exchanging metal ion, which was found to be negligible. The temperature was maintained at 25 °C and the ionic strength of the solutions was kept constant, 0.15 M NaCl. The exchange rates were studied in the pH range 3.0–5.0. For keeping the pH values constant, 1,4-dimethylpiperazine buffer (25 mM) was used. The pseudo-first-order rate constants (k_d) were calculated by fitting the absorbance data with the use of the following equation:

$$A_t = (A_0 - A_e)e^{-k_d t} + A_e \quad (4)$$

where A_t, A_0, and A_e were the absorbance at time t, at the start and at equilibrium of the reactions, respectively. The calculations were performed by using the computer program Micromath Scientist, version 2.0 (Salt Lake City, UT, USA).

MR phantom imaging: ^1H phantom MR images were recorded on a series of Eppendorf tubes containing different dilutions of **GdL**[4] and DOTAREM (**GdDOTA**) in 150 μL of MOPS buffered H_2O (pH 7.4, 0.1 M) at 0, 10, 20, 40, and 80 μM. The images were recorded at 21 °C using 7 T Bruker BioSpec 70/30 USR Preclinical MRI system using a ^1H/volume transmit–receive coil tuned to the proton resonance (300.3 MHz). The map was obtained from a set of inversion-recovery SE measurements (adiabatic 180° pulse with inversion time TI = 23, 50, 150, 250, 500, 750, 1000, 1500, 2000, 2500, 3500, 5000 ms, TE/TR = 10.7/6000 ms, flip angle = 90/180°, effective spectral width 50 kHz, matrix size = 300×300, voxel size 0.2×0.2×2 mm^3, FOV: 6×6 cm). The included T_1 maps show the results obtained by voxel wise nonlinear least-squares fitting of the proton signal, using the Levenberg–Marquardt steepest descent algorithm implemented in MATLAB, version 7.10 (MathWorks Inc., Natick, USA). ^{19}F MR phantom images were recorded on a series of Eppendorf tubes containing different dilutions of **GdL**[4] and **YbL**[4] in 150 μL of MOPS buffered H_2O (pH 7.4, 0.1 M) at 1.0, 2.0, 3.5, and 5.0 mM, on the above scanner equipped with a BGA-9S gradient insert using a dual $^1H/^{19}F$ single loop surface coil (282.56 MHz for ^{19}F). For **YbL**[4] ^{19}F images were acquired by a FLASH sequence with TE/TR = 3.5/45 ms, flip angle = 30°, effective spectral width 10 kHz, 2500 averages, 60 min acquisition time, matrix size = 32×32, voxel size 1×1×5 mm^3, FOV: 3.2×3.2 cm. For **GdL**[4] the parameters used for FLASH were: TE/TR = 2.67/7.48 ms, flip angle = 84.5°, effective spectral width 17.5 kHz, 15000 averages, 60 min acquisition time, matrix size = 32×32, voxel size 1×1×5 mm^3, FOV: 3.2×3.2 cm. For **GdL**[4] ^{19}F MRI was also made using a FISP sequence with TE/TR = 1.2/2.3 ms, flip angle = 60°, effective spectral width 40 kHz, 5000 averages, 60 min acquisition time, matrix size = 64×64, voxel size 1×1×5 mm^3, FOV: 6.4×6.4 cm. For the lower concentrations of **GdL**[4] shown in Figure 9, the sequence parameters for FISP were TE/TR = 0.9/1.8 ms, flip angle = 88°, effective spectral width 29.8 kHz, 44000 averages, 60 min acquisition time, matrix size = 64×64, voxel size 1×1×5 mm^3, FOV: 6.4×6.4 cm. A region-of-interest was placed outside the phantoms to determine the Rayleigh corrected noise level that was used for calculating the SNR of the ^{19}F MR images. The ^1H relaxation rates were quantified from a set of single slice spin echo MR image using the same double tuned coil as for ^{19}F MRI (Figure 9) with a TE/TR = 10.7/6000 ms, flip angle = 90°, effective spectral width 50 kHz, 1 average, 20 min acquisition time, matrix size = 320×320, voxel size 0.1×0.1×2 mm^3, FOV: 3.2×3.2 cm. A slab-selective (6 mm thick) 180° inversion pulse was used with the following inversion times: 23/50/150/250/500/750/1000/1500/2000/2500/3500/5000 ms. Nonlinear least-squares fitting of the modulus data was performed voxel wise according to: $S = S_0(1-\alpha\cdot e^{-R2\cdot TI})$ using the double-fit-

ting algorithm minimizing chi-square.[58] The α factor is 2 if a perfect inversion is obtained. Across the imaged slice this factor was: 2 ± 0.03. MRI data were reconstructed on the scanner and analyzed with home-written MATLAB code (v. 7.10, Mathworks Inc., Natick, USA).

Acknowledgements

We are thankful to Dr. Sara Di Pinto and Dr. Claudio Cassino for their help with relaxometric measurements, and Dr. Louise Natrajan and Dr. Ilgar Mamedov for helpful discussions. Financial support from the Max-Planck Society and the German Research Foundation (DFG, grant No. AN 716/2-1) is gratefully acknowledged. The European COST Action D38 "Metal-Based Systems for Molecular Imaging Applications", TD1004 "Theranostics Imaging and Therapy: An Action To Develop Novel Nanosized Systems For Imaging-Guided Drug Delivery", CM1006 "EUFEN: European F-Element Network", the Hungarian Scientific Research Foundation (OTKA PD-83253 and K-84291), the TÁMOP-4.2.2A-11/1/KONV-2012-0043 and TÁMOP-4.2.2/B-10/1-2010-0024 projects implemented through the New Hungary Development Plan, co-financed by the European Social Fund and the European Regional Development Fund, and the Italy–Hungary Intergovernmental S&T Cooperation Program (HU11 MO2-TET_10-1-2011-0202) are also acknowledged.

[1] J. K. Willmann, N. van Bruggen, L. M. Dinkelborg, S. S. Gambhir, *Nat. Rev. Drug Discovery* **2008**, *7*, 591–607.
[2] M. M. J. Modo, J. W. M. Bulte, *Molecular and Cellular MR Imaging*, CRC, Boca Raton, **2007**, p. 421.
[3] N. Bloembergen, L. O. Morgan, *J. Chem. Phys.* **1961**, *34*, 842.
[4] a) A. E. Merbach, E. Toth, *The Chemistry of Contrast Agents in Medical Magnetic Resonance Imaging*, Wiley, Chichester, **2001**; b) P. Caravan, J. J. Ellison, T. J. McMurry, R. B. Lauffer, *Chem. Rev.* **1999**, *99*, 2293–2352.
[5] M. Botta, *Eur. J. Inorg. Chem.* **2000**, 399–407.
[6] P. Lebduskova, P. Hermann, L. Helm, E. Toth, J. Kotek, K. Binnemans, J. Rudovsky, I. Lukes, A. E. Merbach, *Dalton Trans.* **2007**, 493–501.
[7] a) P. Caravan, *Chem. Soc. Rev.* **2006**, *35*, 512–523; b) E. J. Werner, A. Datta, C. J. Jocher, K. N. Raymond, *Angew. Chem.* **2008**, *120*, 8696–8709; *Angew. Chem. Int. Ed.* **2008**, *47*, 8568–8580.
[8] M. Srinivas, A. Heerschap, E. T. Ahrens, C. G. Figdor, I. J. M. d. Vries, *Trends Biotechnol.* **2010**, *28*, 363–370.
[9] a) J. Ruiz-Cabello, P. Walczak, D. A. Kedziorek, V. P. Chacko, A. H. Schmieder, S. A. Wickline, G. M. Lanza, J. W. M. Bulte, *Magn. Reson. Med.* **2008**, *60*, 1506–1511; b) E. T. Ahrens, R. Flores, H. Y. Xu, P. A. Morel, *Nat. Biotechnol.* **2005**, *23*, 983–987.
[10] a) K. J. Thurecht, I. Blakey, H. Peng, O. Squires, S. Hsu, C. Alexander, A. K. Whittaker, *J. Am. Chem. Soc.* **2010**, *132*, 5336–5337; b) M. Ogawa, S. Nitahara, H. Aoki, S. Ito, M. Narazaki, T. Matsuda, *Macromol. Chem. Phys.* **2010**, *211*, 1602–1609.
[11] a) L. Helm, *Prog. Nucl. Magn. Reson. Spectrosc.* **2006**, *49*, 45–64; b) P. Harvey, I. Kuprov, D. Parker, *Eur. J. Inorg. Chem.* **2012**, 2015–2022.
[12] a) S. Mizukami, R. Takikawa, F. Sugihara, Y. Hori, H. Tochio, M. Walchli, M. Shirakawa, K. Kikuchi, *J. Am. Chem. Soc.* **2008**, *130*, 794–795; b) S. Mizukami, H. Matsushita, R. Takikawa, F. Sugihara, M. Shirakawa, K. Kikuchi, *Chem. Sci.* **2011**, *2*, 1151–1155.
[13] K. H. Chalmers, A. M. Kenwright, D. Parker, A. M. Blamire, *Magn. Reson. Med.* **2011**, *66*, 931–936.
[14] a) S. A. Anderson, R. K. Rader, W. F. Westlin, C. Null, D. Jackson, G. M. Lanza, S. A. Wickline, J. J. Kotyk, *Magn. Reson. Med.* **2000**, *44*, 433–439; b) K. C. Partlow, J. Chen, J. A. Brant, A. M. Neubauer, T. E. Meyerrose, M. H. Creer, J. A. Nolta, S. D. Caruthers, G. M. Lanza, S. A. Wickline, *FASEB J.* **2007**, *21*, 1647–1654.
[15] E. Gianolio, R. Napolitano, F. Fedeli, F. Arena, S. Aime, *Chem. Commun.* **2009**, 6044–6046.
[16] M. P. Placidi, J. Engelmann, L. S. Natrajan, N. K. Logothetis, G. Angelovski, *Chem. Commun.* **2011**, *47*, 11534–11536.
[17] K. H. Chalmers, M. Botta, D. Parker, *Dalton Trans.* **2011**, *40*, 904–913.
[18] a) J. C. G. Bunzli, P. Froidevaux, J. M. Harrowfield, *Inorg. Chem.* **1993**, *32*, 3306–3311; b) W. D. Horrocks, J. P. Bolender, W. D. Smith, R. M. Supkowski, *J. Am. Chem. Soc.* **1997**, *119*, 5972–5973.
[19] A. Beeby, I. M. Clarkson, R. S. Dickins, S. Faulkner, D. Parker, L. Royle, A. S. de Sousa, J. A. G. Williams, M. Woods, *J. Chem. Soc. Perkin Trans. 2* **1999**, 493–503.
[20] P. Atkinson, B. S. Murray, D. Parker, *Org. Biomol. Chem.* **2006**, *4*, 3166–3171.
[21] a) S. Aime, M. Botta, D. Parker, J. A. G. Williams, *J. Chem. Soc. Dalton Trans.* **1996**, 17–23; b) J. Rudovsky, P. Cigler, J. Kotek, P. Hermann, P. Vojtisek, I. Lukes, J. A. Peters, L. Vander Elst, R. N. Muller, *Chem. Eur. J.* **2005**, *11*, 2373–2384; c) J. Rudovsky, M. Botta, P. Hermann, A. Koridze, S. Aime, *Dalton Trans.* **2006**, 2323–2333.
[22] a) S. Aime, M. Botta, E. Garino, S. G. Crich, G. Giovenzana, R. Pagliarin, G. Palmisano, M. Sisti, *Chem. Eur. J.* **2000**, *6*, 2609–2617; b) J. B. Livramento, A. Sour, A. Borel, A. E. Merbach, V. Toth, *Chem. Eur. J.* **2006**, *12*, 989–1003.
[23] a) S. H. Koenig, R. D. Brown, *Prog. Nucl. Magn. Reson. Spectrosc.* **1990**, *22*, 487–567; b) D. H. Powell, O. M. Ni Dhubhghaill, D. Pubanz, L. Helm, Y. S. Lebedev, W. Schlaepfer, A. E. Merbach, *J. Am. Chem. Soc.* **1996**, *118*, 9333–9346.
[24] S. Aime, M. Botta, M. Fasano, E. Terreno, *Chem. Soc. Rev.* **1998**, *27*, 19–29.
[25] S. Aime, M. Botta, S. G. Crich, G. Giovenzana, R. Pagliarin, M. Sisti, E. Terreno, *Magn. Reson. Chem.* **1998**, *36*, S200–S208.
[26] D. Messeri, M. P. Lowe, D. Parker, M. Botta, *Chem. Commun.* **2001**, 2742–2743.
[27] a) A. Datta, J. M. Hooker, M. Botta, M. B. Francis, S. Aime, K. N. Raymond, *J. Am. Chem. Soc.* **2008**, *130*, 2546–2552; b) Z. Jászberényi, L. Moriggi, P. Schmidt, C. Weidensteiner, R. Kneuer, A. E. Merbach, L. Helm, E. Toth, *J. Biol. Inorg. Chem.* **2007**, *12*, 406–420; c) G. M. Nicolle, E. Toth, H. Schmitt-Willich, B. Raduchel, A. E. Merbach, *Chem. Eur. J.* **2002**, *8*, 1040–1048.
[28] J. Costa, E. Balogh, V. Turcry, R. Tripier, M. Le Baccon, F. Chuburu, H. Handel, L. Helm, E. Toth, A. E. Merbach, *Chem. Eur. J.* **2006**, *12*, 6841–6851.
[29] a) T. J. Swift, R. E. Connick, *J. Chem. Phys.* **1962**, *37*, 307–320; b) K. Micskei, L. Helm, E. Brucher, A. E. Merbach, *Inorg. Chem.* **1993**, *32*, 3844–3850.
[30] J. F. Desreux, E. Merciny, M. F. Loncin, *Inorg. Chem.* **1981**, *20*, 987–991.
[31] R. G. Franz, *AAPS PharmSciTech* **2001**, *3*, E10.
[32] Z. Baranyai, Z. Palinkas, F. Uggeri, E. Brücher, *Eur. J. Inorg. Chem.* **2010**, 1948–1956.
[33] W. P. Cacheris, S. K. Nickle, A. D. Sherry, *Inorg. Chem.* **1987**, *26*, 958–960.
[34] I. Mamedov, P. Táborský, P. Lubal, S. Laurent, L. V. Elst, H. A. Mayer, N. K. Logothetis, G. Angelovski, *Eur. J. Inorg. Chem.* **2009**, 3298–3306.
[35] a) M. Forsterova, I. Svobodova, P. Lubal, P. Taborsky, J. Kotek, P. Hermann, I. Lukes, *Dalton Trans.* **2007**, 535–549; b) S. L. Wu, W. D. Horrocks, *Inorg. Chem.* **1995**, *34*, 3724–3732.
[36] a) J. Moreau, E. Guillon, J.-C. Pierrard, J. Rimbault, M. Port, M. Aplincourt, *Chem. Eur. J.* **2004**, *10*, 5218–5232; b) E. Toth, E. Brucher, I. Lazar, I. Toth, *Inorg. Chem.* **1994**, *33*, 4070–4076.
[37] A. Bianchi, L. Calabi, F. Corana, S. Fontana, P. Losi, A. Maiocchi, L. Paleari, B. Valtancoli, *Coord. Chem. Rev.* **2000**, *204*, 309–393.
[38] H.-Z. Cai, T. A. Kaden, *Helv. Chim. Acta* **1994**, *77*, 383–398.
[39] J. Kotek, F. K. Kalman, P. Hermann, E. Brucher, K. Binnemans, I. Lukes, *Eur. J. Inorg. Chem.* **2006**, 1976–1986.
[40] Z. Baranyai, Z. Pálinkás, F. Uggeri, A. Maiocchi, S. Aime, E. Brücher, *Chem. Eur. J.* **2012**, *18*, 16426–16435.
[41] L. Sarka, L. Burai, R. Király, L. Zékány, E. Brücher, *J. Inorg. Biochem.* **2002**, *91*, 320–326.
[42] K. Kumar, T. Jin, X. Wang, J. F. Desreux, M. F. Tweedle, *Inorg. Chem.* **1994**, *33*, 3823–3829.

[43] F. K. Kálmán, Z. Baranyai, I. Tóth, I. Bányai, R. Király, E. Brücher, S. Aime, X. Sun, A. D. Sherry, Z. Kovács, *Inorg. Chem.* **2008**, *47*, 3851–3862.
[44] a) J. A. Peters, J. Huskens, D. J. Raber, *Prog. Nucl. Magn. Reson. Spectrosc.* **1996**, *28*, 283–350; b) D. Parker, R. S. Dickins, H. Puschmann, C. Crossland, J. A. K. Howard, *Chem. Rev.* **2002**, *102*, 1977–2010.
[45] C. Platas-Iglesias, *Eur. J. Inorg. Chem.* **2012**, 2023–2033.
[46] a) S. Aime, M. Botta, G. Ermondi, *Inorg. Chem.* **1992**, *31*, 4291–4299; b) S. Aime, M. Botta, M. Fasano, M. P. M. Marques, C. F. G. C. Geraldes, D. Pubanz, A. E. Merbach, *Inorg. Chem.* **1997**, *36*, 2059–2068.
[47] a) M. Jauregui, W. S. Perry, C. Allain, L. R. Vidler, M. C. Willis, A. M. Kenwright, J. S. Snaith, G. J. Stasiuk, M. P. Lowe, S. Faulkner, *Dalton Trans.* **2009**, 6283–6285; b) J. P. André, C. F. G. C. Geraldes, J. A. Martins, A. E. Merbach, M. I. M. Prata, A. C. Santos, J. J. P. de Lima, E. Toth, *Chem. Eur. J.* **2004**, *10*, 5804–5816.
[48] M. Woods, S. Aime, M. Botta, J. A. K. Howard, J. M. Moloney, M. Navet, D. Parker, M. Port, O. Rousseaux, *J. Am. Chem. Soc.* **2000**, *122*, 9781–9792.
[49] C. S. Johnson, *Prog. Nucl. Magn. Reson. Spectrosc.* **1999**, *34*, 203–256.
[50] J. Henig, I. Mamedov, P. Fouskova, E. Tóth, N. K. Logothetis, G. Angelovski, H. A. Mayer, *Inorg. Chem.* **2011**, *50*, 6472–6481.
[51] R. Freeman, H. D. W. Hill, *J. Magn. Reson.* **1971**, *4*, 366–383.
[52] M. Botta, L. Tei, *Eur. J. Inorg. Chem.* **2012**, 1945–1960.
[53] A. Dadabhoy, S. Faulkner, P. G. Sammes, *J. Chem. Soc. Perkin Trans. 2* **2002**, 348–357.
[54] D. M. Corsi, C. Platas-Iglesias, H. van Bekkum, J. A. Peters, *Magn. Reson. Chem.* **2001**, *39*, 723–726.
[55] R. Delgado, J. J. R. F. Dasilva, *Talanta* **1982**, *29*, 815–822.
[56] H. M. Irving, M. G. Miles, L. D. Pettit, *Anal. Chim. Acta* **1967**, *38*, 475–488.
[57] D. J. Leggett, *Computational Methods for the Determination of Formation Constants*, Plenum, New York, **1985**.
[58] D. R. Messroghli, A. Rudolph, H. Abdel-Aty, R. Wassmuth, T. Kuhne, R. Dietz, J. Schulz-Menger, *BMC Med. Imaging* **2010**, *10*, 16.

Received: February 26, 2013
Published online: ■■ ▮▮, 0000

